Light-induced Conformational Changes in the Photosynthetic Reaction Center from *Rhodobacter sphaeroides*

Sasmit S. Deshmukh

A Thesis

in

The Department

of

Chemistry and Biochemistry

Presented in Partial Fulfillment of the Requirements
for the Degree of Master of Science (Chemistry) at
Concordia University
Montreal, Quebec, Canada

April 2009

Your file Votre référence
ISBN: 978-0-494-63275-8
Our file Notre référence
ISBN: 978-0-494-63275-8

ABSTRACT

Light-induced Conformational Changes in the Photosynthetic Reaction Center from *Rhodobacter sphaeroides*

Sasmit S. Deshmukh

The photosynthetic reaction center (RC) from purple photosynthetic bacteria is a membrane-bound protein-pigment complex that serves as an excellent model for studying biological energy conversion. This energy conversion takes place by electron transfer reactions, which occur within the protein and are often coupled to conformational changes. In order to study these conformational changes, recovery of the oxidized bacteriochlorophyll dimer, from the RC of the purple photosynthetic bacterium *Rhodobacter sphaeroides,* to its original state was measured by light-minus-dark optical difference spectroscopy. Laser flash excitation generated an electron transfer that takes place across the membrane; creating the primary charge-separated state with a lifetime of 100 ms. Prolonged illumination induced subsequent conformational rearrangements in the RC protein complex which result in lifetimes of the same charge-separated state that are significantly different from that measured after flash excitation. The structural details of the conformational rearrangements on the molecular level will be discussed. The conformational changes were sensitive to duration and wavelength of illumination, pH, temperature, hydrophobic environment (liposome or detergent), head-group charge of the detergent, and presence of a bound metal ion. By systematically varying these parameters, we were able to extend the lifetime of the charge-separated state up to 21 mins. Based on these results, our goal is to utilize the bacterial RC protein complex as a biocapacitor, since the positive and negative charges are separated by a hydrophobic core of the protein with a low dielectric constant. This biocapacitor can be discharged rapidly by inducing pH jump.

Acknowledgements

I would like to thank my supervisor, Dr. Laszlo Kalman for all his guidance and valuable help throughout the project. I would also like to thank my committee members Dr. Cameron Skinner, Dr. Christine DeWolf, and Dr. Paul Joyce for their valuable discussion and advises. I am grateful to Dr. James P. Allen and JoAnn C. Williams (coauthors of the prepared manuscript) for providing mutants. I am thankful to my colleague Kai Tang for his help in liposome measurements.

Table of Contents

List of Figures

List of Tables

Abbreviations

BChl	Bacteriochlorophyll monomer
$(BChl)_2$	Bacteriochlorophyll dimer
Bpheo	Bacteriopheophytine
BRC	Bacterial reaction center
BWHM	Bandwidth at half maxima
c.m.c.	Critical micelle concentration
cyt c_2	Cytochrome c_2
cyt bc_1	Cytochrome bc_1
DLPC	1, 2-Dilauroyl-sn-Glycero-3-phosphocholine
EDTA	Ethylene diamine tetraacetic acid
LDAO	Lauryl dimethyl amine-n-oxide
LFP	Laser flash photolysis
P	Primary donor or bacteriochlorophyll dimer
PS II	Photosystem II
Q_A	Primary quinone
Q_B	Secondary quinone
Rb	Rhodobacter
RC	Reaction center

Chapter 1

Introduction

1.1 Basic principles of photosynthesis

Photosynthesis is the primary solar energy conversion and every aspect of life currently on the Earth is dependent on it. Oxygen producing photosynthesis made, and makes, life possible for aerobic organisms. Essentially all of our food is related to photosynthesis and all of our current fossil fuels are the products of photosynthetic activities that occurred many millions of years ago. The first step of the conversion of light energy into chemical energy, is accomplished in pigment-protein complexes, termed reaction centers in green plants, algae, cyanobacteria and purple nonsulfur bacteria. In green plants and cyanobacteria water is used as the electron donor and carbon dioxide is the carbon source in the conversion of light energy into chemical energy, while sugars are synthesized and oxygen as a byproduct is released (Figure 1.1). In algae, cyanobacteria and chloroplasts of green plants, Photosystem II (PS II) reaction center is responsible for splitting the water into molecular oxygen, electrons and protons. Oxygen is released to the atmosphere while the electrons and protons are used to reduce plastoquinones. These protons also create a proton gradient across the membrane to drive ATP synthesis, which in turn can catalytically empower many biochemical reactions ultimately leading to the synthesis of glucose [1].

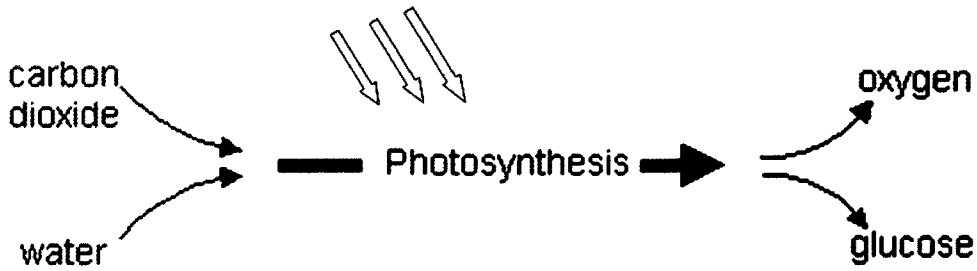

Light energy ⟶ Chemical energy

Figure 1.1 Photosynthesis. The process of oxygenic photosynthesis, where carbon dioxide and water are converted into oxygen and glucose using the energy of light.

Photosystem II contains three extrinsic proteins that are required exclusively for splitting water. They include a cluster of four manganese ions and two specific tyrosine residues. The manganese cluster acts as a "four electron gate" that releases four oxidizing equivalents in the form of an oxygen molecule as a result of a cyclic four step electron transfer process to the primary electron donor (P680), which is mediated by the secondary electron donor, a tyrosine residue [1]. The sequence of electron transfer can be given as:

H_2O ⟶ Manganese cluster ⟶ Tyrosine ⟶ Primary donor (P680) ⟶ Bpheo ⟶ Q_A ⟶ Q_B

Bpheo: Pheophytin molecule (The primary electron acceptor)

Q_A and Q_B: Plastoquinones

In the case of bacterial reaction center (BRC), cytochrome c acts as an external electron donor, which re-reduces the primary electron donor. Bacterial photosynthesis does not produce oxygen therefore it is termed anoxygenic photosynthesis. The structural and functional similarities between the evolutionarily related but way more complex PS II and the simpler BRC make the latter an excellent model for studying biological energy conversion.

1.2 Structure of photosynthetic BRC from *Rb. sphaeroides*

The three dimensional structure of the BRC from *Rb. sphaeroides* has been determined by X-ray diffraction at a resolution of 2.8 Å, which is helpful in elucidating the structure-function relationship [2, 3].

The RC from photosynthetic bacteria is an integral membrane protein-pigment complex, with around ~800 amino acid residues, which contains nine cofactors that mediate the primary photochemistry. The RC from the *Rb. sphaeroides* has three protein subunits L- (light), M- (medium) and H- (heavy) as determined from early gel electrophoresis, with molecular masses ~21, ~24, and ~28 kDa respectively. The actual molecular weights were later determined to be incorrect since the mostly polar H-subunit was migrating in the gel slower and that is why it was labeled as heaviest. Actually, it is the lightest one but the names remained. The L- and M- subunits each contain five membrane spanning helices and several helices that do not span the membrane (Figure 1.2A). The H- subunit has one membrane spanning helix and a globular domain on the cytoplasmic side, which

contains one helix that does not span the membrane and several β-sheets. The L- and M- subunits are related to each other by a 2-fold rotational symmetry axis, which is approximately the same as determined for the cofactors. Cofactors are associated with the L- and M-subunits across a two fold symmetry axis, which includes one bacteriochlorophyll dimer (P) composed of two bacteriochlorophylls, two bacteriochlorophyll monomers ($BChl_A$ and $BChl_B$), two bacteriopheophytine ($Bpheo_A$ and $Bpheo_B$), two ubiquinones (Q_A: Primary quinone and Q_B: Secondary quinone), and a non-heme iron (Figure 1.2B). The two fold symmetry axis passes through $(BChl)_2$ and non-heme iron [2, 3].

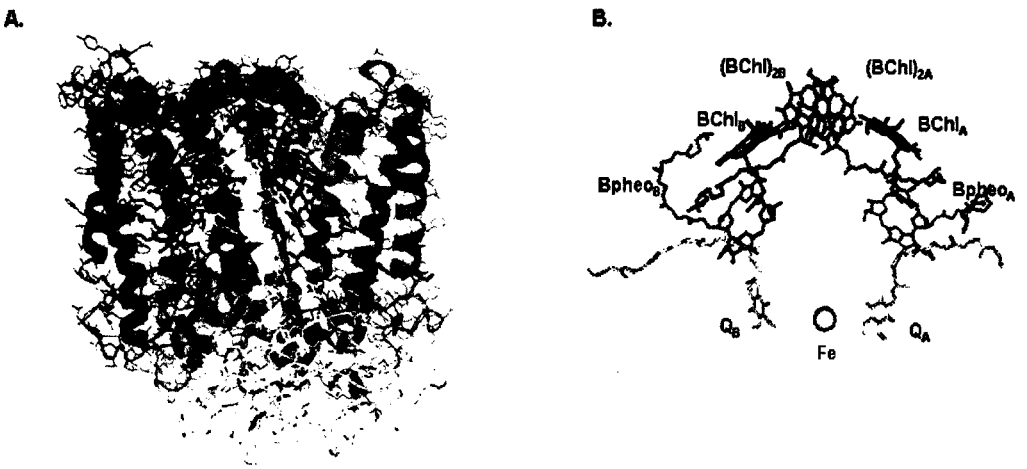

Figure 1.2 Structure of the bacterial reaction center (BRC) from the carotenoidless strain of *Rhodobacter sphaeroides* **A.** The arrangement of protein subunits: L, M, and . The molecules colored RED are the cofactors bound to the protein by noncovalent interactions. **B.** Details of the 9 cofactors of the BRC, which are aligned across the 2-fold symmetric axis passing vertically through the plane of paper from $(BChl)_2$ to non-heme iron (Fe). Cofactors are tightly bound and solvent inaccessible. The periplasmic side of the membrane is near the top and cytoplasmic side is near the bottom of the structure [2, 3]. Figures were prepared by Pymol software from PDB file 4RCR [4].

1.3 Electron transfer process in BRC

Light induced electron transfer takes place from the primary donor (P) to the secondary quinone (Q_B) via a series of intermediate acceptors including bacteriochlorophyll monomer ($BChl_A$), bacteriopheophytine ($Bpheo_A$) and primary quinone (Q_A) (Figure 1.3A). Oxidized dimer (P^+) can be re-reduced by the exogenous electron donor cytochrome c_2 (cyt c_2) then after a second excitation a transfer of a second electron takes place and the secondary quinone can be reduced twice. It accepts two protons in this process from the cytoplasmic side to become quinol (Q_BH_2). The primary quinone (Q_A^-) serves as an electron donor to Q_B. Despite the apparent two fold symmetry, Q_A and Q_B have different properties: Q_A is tightly bound and functions as a one-electron acceptor in the primary photochemistry while Q_B is more weakly bound and functions as a two-electron, two-proton acceptor that dissociates after reduction [5] and shuttles protons and electrons across the membrane. The first proton transfer to Q_B is coupled with the second electron transfer from Q_A^- to Q_B^-. The pathway of proton transfer to Q_B deduced from mutagenesis experiments [6-12] indicates that the first proton, $H^+(1)$, is bound by the carbonyl oxygen of Q_B , which is distal to the iron atom and the second proton, $H^+(2)$, is bound by the carbonyl oxygen proximal to the iron atom [13].

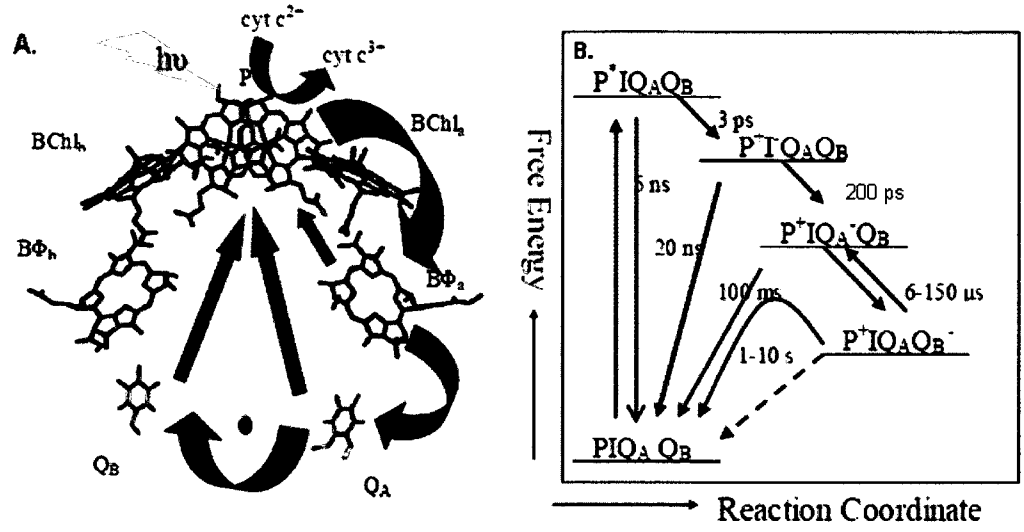

Figure 1.3 Light-induced electron transfer process in photosynthetic bacterial reaction centers. A. The pathway of the light induced forward electron transfer indicated by the green arrows and the red arrows represent the charge recombination. **B.** The energy levels of various redox states formed during the electron transfer process. As in panel A, the green arrows show the forward electron transfer while the red arrows show the charge recombination processes. P^+I^- represents intermediate charge separated states involving the dimer and the pheophytine. Indicated times represent the lifetimes of the redox states in the forward electron transfer and in the charge recombination.

Free energy levels suggest that forward electron transfer is favorable to the charge recombination from intermediate state because it is orders of magnitude faster (Figure 1.3B). The electron transfer is highly unidirectional proceeding via the A-branch because there are three natural lipids found in the RC (Figure 1.4) namely glycolipid, phospholipid and cardiolipin [14]. The lipid composition in natural cell membrane environment depends on growth condition of the bacterium, for example oxygen level [14]. Interaction of these lipids with the cofactors alters the energy levels of the charge separated state (Figure 1.4) compelling highly

unidirectional electron transfers. The electron transfer from Q_A to Q_B takes place due to the different amino acid surroundings of Q_A and Q_B respectively. This electron transfer is attributed by a conformational gating step, which causes the movement of Q_B from distal to proximal position [15].

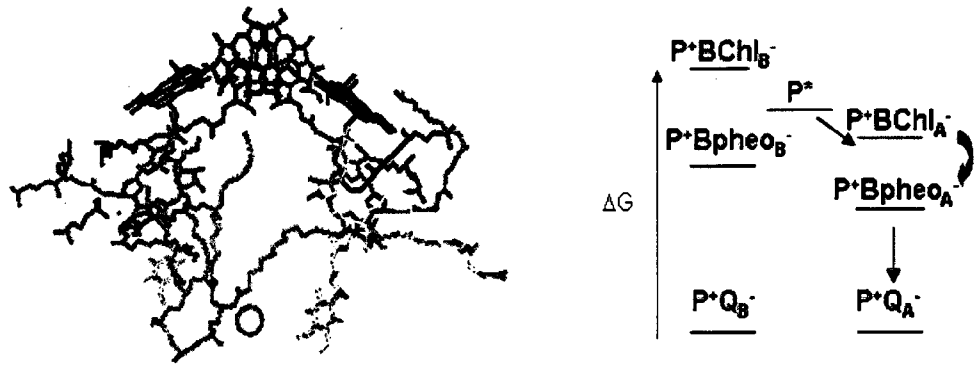

Figure 1.4 Position of the integrated lipids with nearby cofactors and their influence on the energetics of the unidirectional electron transfer. A Glycolipid (yellow molecule) molecule binds near $BChl_A$. The phospholipid phosphatidylcholine binds near the $Bpheo_B$. The cardiolipin (cyan molecule) binds near M- subunit but does not interact directly with cofactors. Due to interactions of these lipids the energy levels of the cofactors are altered. As a result, the electron transfer proceeds along the "A- branch" of the cofeactors only.

1.4 Generation of the proton electrochemical gradient in the membrane of *Rb. sphaeroides*

In the natural membrane environment the transmembrane electron transfer takes place upon light excitation. After accepting two electrons and two protons, the

secondary quinone (Q_B) becomes a quinol (Q_BH_2). Then this quinol will be replaced by a new quinone molecule from the quinone pool and the quinol becomes oxidized by cytochrome bc_1 complex. In this process protons are released to periplasmic side, which can create a proton electrochemical gradient to drive the ATP synthase [16]. Electrons can be transferred from cyt bc_1 complex to RC through the mobile electron carrier cyt c_2 (Figure 1.5).

To study the BRC in detail, it needs to be isolated from the natural membrane environment because studies of BRCs in membrane fragments (chromatophores) using optical techniques are hampered by the presence of light harvesting (LH) complex pigments and therefore are most often performed on isolated, detergent solubilized BRC complexes [17].

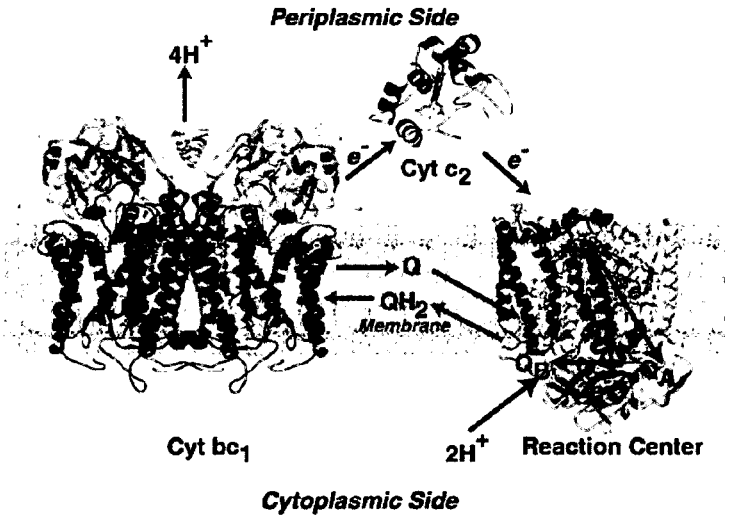

Figure 1.5 The photosynthetic electron transfer cycle in the membrane of the photosynthetic bacterium *Rb. sphaeroides*. Light induces transfer of an electron from the primary donor, $(BChl)_2$ of RC through a series of electron acceptors to reduce a reversibly bound Q_B. Reduced quinone is released by the RC and gets re-oxidized by cytochrome bc_1 complex [18] pumping protons across the membrane. The mobile electron carrier cyt c_2 accepts an electron from cytochrome bc_1 complex and migrates to the RC to transfer an electron to re-reduce the primary donor.

1.5 Hydrophobic environment of the reaction center protein

Bacterial reaction center is an integral membrane protein and thus it has to be in a amphyphilic environment in order to function. Therefore after extracting BRC's from the natural membrane environment, it has to be incorporated in detergent micelles that are substitutes for the membrane. The BRC has a large hydrophobic region and as a result is not soluble in water. Solubilization and incorporation of isolated BRC is achieved in detergent micelles, which encompasses its hydrophobic region (Figure 1.6). The detergent forms a belt like structure surrounding the hydrophobic part of the BRC and has a hydrophobic thickness of ~23 Å that is about 5 Å thinner than the hydrophobic transmembrane helices as both determined by neutron diffraction experiments [19].

For solubilization, the detergent concentration always has to be higher than the critical micelle concentration (c.m.c.). The c.m.c is defined as the concentration above which micelles are spontaneously formed in the bulk solution. When detergent is dissolved in water, it concentrates at the surface, where by orienting so that their hydrophobic groups are directed away from the solvent, the free energy of the solution is minimized.

Above the c.m.c., this can be achieved by forming micelles, where the detergent hydrophobic tails are directed towards the interior of the cluster and the hydrophilic groups are directed towards the solvent [20]. These detergent micelles

then cover the hydrophobic region of the protein and help to disperse it in aqueous environment.

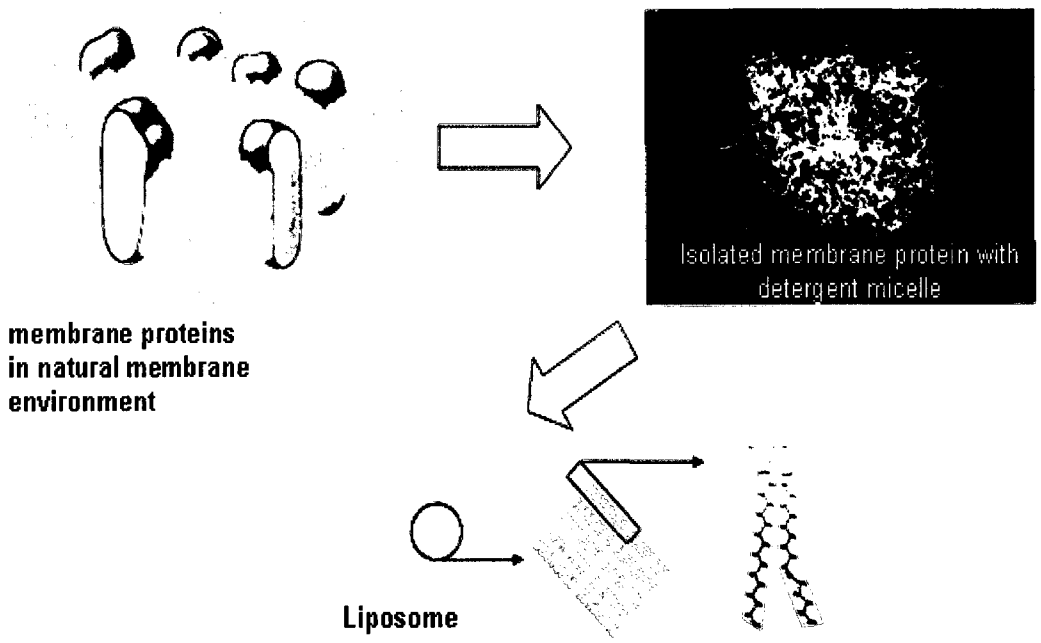

Figure 1.6 BRC in the natural membrane environment, in detergent micelles, and in liposomes. BRC's in natural membrane environment (pink) can be isolated and incorporated into detergent micelles (blue). These detergent micelles form a belt like structure around the hydrophobic environment of the BRC. To mimic, and to some extent restore, the hydrophobic environment of the membrane, the BRCs can be incorporated into liposomes by removing detergent micelles. Figure was modified from reference 19.

In this project, lauryldimethylamine-oxide (zwitterioninc at pH 7 and above [21] with pKa~ 6.6 [22]) and Triton X-100 (non-ionic) detergents have been used to disperse the BRC protein having c.m.c. of 0.023% and 0.033% in the solution respectively.

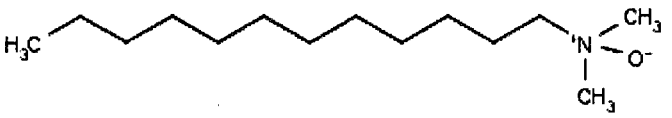

lauryldimethylamine-oxide (LDAO) (zwitterionic detergent)

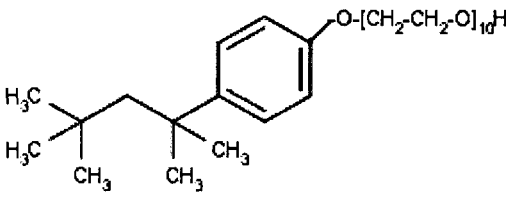

Triton X-100 (non-ionic detergent)

Changes in temperature, detergent concentration, and structural groups in the detergent may all cause change in the size, shape, and aggregation number of the micelle.

Ionic detergents show aggregation numbers, the number of molecules present in a micelle, of less than 100 in aqueous solutions of low ionic strength and these vary only slightly with the detergent concentration. This is indicative of spherical micelle formation. At high ionic strength (20 mM and above), however, the aggregation number increases sharply with detergent concentration, with formation of cylindrical micelles. This means a decrease in the ionic strength of the solution and a resulting increase in the value of surface area of head group due to charge-charge interaction, producing smaller aggregation number. Aggregation numbers of LDAO and Triton X-100 detergents are 70 and 140 respectively in solutions without salt [20].

An increase in the temperature appears to cause a small decrease in the aggregation number in aqueous medium, presumably because the area of the head-groups is increased due to thermal agitation [20].

The structure of the detergent affects the value of the c.m.c. in aqueous media. The c.m.c. decreases as the number of carbon atoms in the hydrophobic group increases. For non-ionic and zwitterionic detergents, the decrease in c.m.c. with increase in the hydrophobic group is somewhat larger; an increase by two methyl units reduces the c.m.c. by about one order of magnitude. A phenyl group that is part of a hydrophobic group with a terminal hydrophilic group is equivalent to about three and one-half methyl groups. When the number of carbon atoms in a straight-chain hydrophobic group exceeds 18, the c.m.c may remain substantially unchanged with further increase in the chain length. This may be due to the coiling of these long chains in water [20].

1.6 Interaction between the membrane proteins and the surrounding environment (hydrophobic mismatch)

After isolation and purification, BRC's can be incorporated into different detergent micelles or different liposomes (Figure 1.7). Liposomes are closed assemblies formed by bilayers of lipid molecules. In BRC detergent micelles the hydrophobic alkyl chains are pointing towards the hydrophobic part of the BRC and hydrophilic head groups points at the external surface of the detergent belt (Figure 1.7C). If we have more than one RC in the system then the detergent belt

of one RC may interact with the detergent belt of other RC (Figure 1.7A). Depending on the hydrophobic environment BRCs have different features as far as electron transfer is concerned. For example, charge recombination from Q_B in detergent micelles takes place in ~1 s while it takes ~10 s in case of liposomes upon flash excitation [23, 24].

Hydrophobic interactions play a major role in stabilizing membrane proteins. BRC incorporated in liposomes, lipid bilayers, or detergent micelles are surrounded by the hydrophobic tails of the lipids or detergent molecules covering the hydrophobic part of the BRC (~24-28 Å) (Figure 1.7). Hydrophobic mismatch could occur if the hydrophobic length of the BRC is shorter or longer as compared to the hydrophobic tail length of the surrounding environment. This disorder can be minimized by two ways:

1. Compensation from the lipid or detergent, and
2. Compensation from the protein.

1.6.1 Compensation from the lipid or detergent

If the hydrophobic tail length of the lipid is shorter or longer than the hydrophobic length of the protein then the lipid has to extend, or compress, in order to minimize the hydrophobic mismatch (Figure 1.8). Compensation from the detergent micelles in proteins dispersed in detergents are also expected but the flexibility in that matter of the detergent molecules is generally less than the

lipids. If the hydrophobic length of the lipid matches with the hydrophobic length of the protein then that is the most favorable situation.

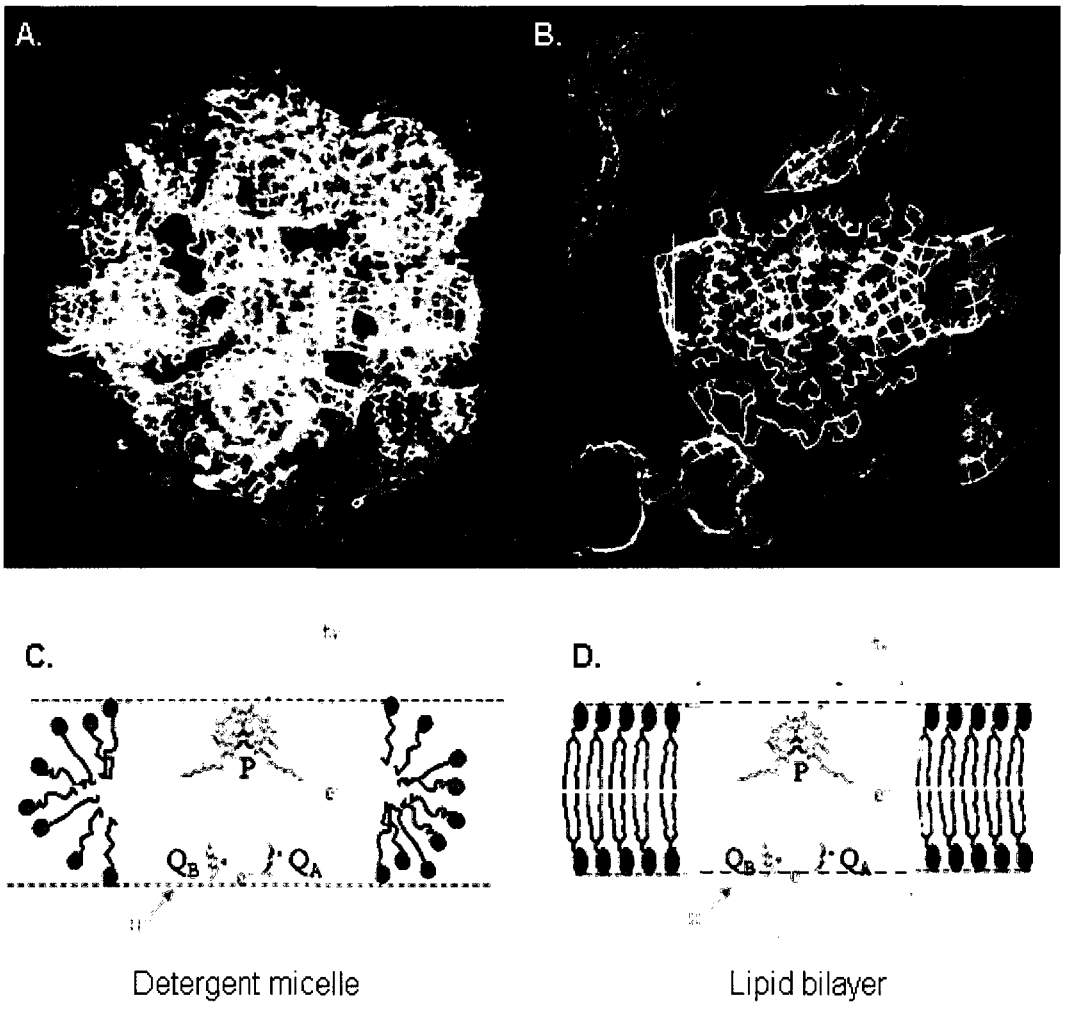

Figure 1.7 Protein-detergent interactions in BRC from *Rb. sphaeroides* A. Alignment of interacting detergent rings (blue) and BRC molecules, which are surrounded by these rings (pink) **B.** Detergent forms belt like structure (blue) around BRC (yellow) where thickness of the detergent belt is 5 Å smaller than the thickness of hydrophobic part of the BRC (23 Å) [19]. **C.** BRC incorporated in detergent micelles. **D.** BRC incorporated in lipid bilayer.

During hydrophobic mismatch lipid has to undergo a large perturbation near the BRC protein in order to minimize the hydrophobic mismatch. This perturbation extends over a few lipid molecules around the BRC protein and recovers back to its normal thickness following an exponential function [25]. These local perturbations in acyl chain causes an overall upward or downward shift (ΔT) in the phase transition temperature of the lipid. Lipids have gel and liquid crystalline (lamellar) phases. In the gel phase the acyl chains are stretched and rigid while in the liquid crystalline phase the acyl chains are fluidic and randomly oriented. The temperature at which the lipid undergoes physical change from liquid crystalline phase to the gel phase is called the transition temperature [26].

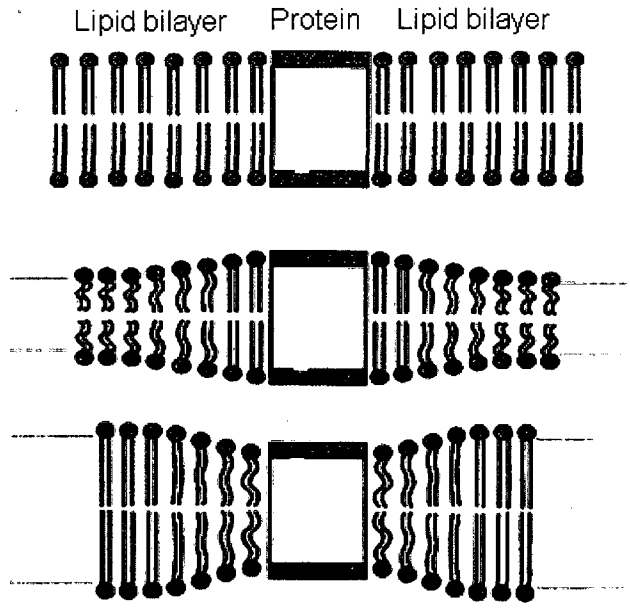

Figure 1.8 Compensation for hydrophobic mismatch from lipid. **A.** Hydrophobic length of the protein matches exactly with the hydrophobic chain length of the lipid. **B.** Hydrophobic length of the protein is larger than that of the acyl chain length of the lipid, and compensation occurs by extending the acyl chain length. **C.** Hydrophobic length of the protein is smaller than that of the acyl chain length of the lipid, then compensation occurs by compressing the acyl chain length [27].

1.6.2. Compensation from the protein

The proteins also undergo conformational changes to compensate for the hydrophobic mismatch. The protein has to tilt in such a way that the hydrophobic α-helices interact with the hydrophobic tails of the lipid bilayer (Figure 1.9), which causes tilted α-helices. In the X-ray structure of the BRC from *Rb. sphaeroides,* it was found that the α-helices were slightly tilted due to structural constraints indicating that compensation to minimize hydrophobic mismatch with detergent micelle environment [28, 29]. The average tilt angle is 22° for transmembrane helices determined from crystal structures reported for membrane proteins [29]. There is a certain critical angle beyond the α-helices cannot tilt further to avoid hydrophobic mismatch and the protein aggregates. Due to limitation for tilt, hydrophobic mismatch cannot be avoided completely by tilting. Aggregation causes loss in the function of the protein. On the other hand it can be utilized for protein purification, namely selective precipitation of proteins from a mixture.

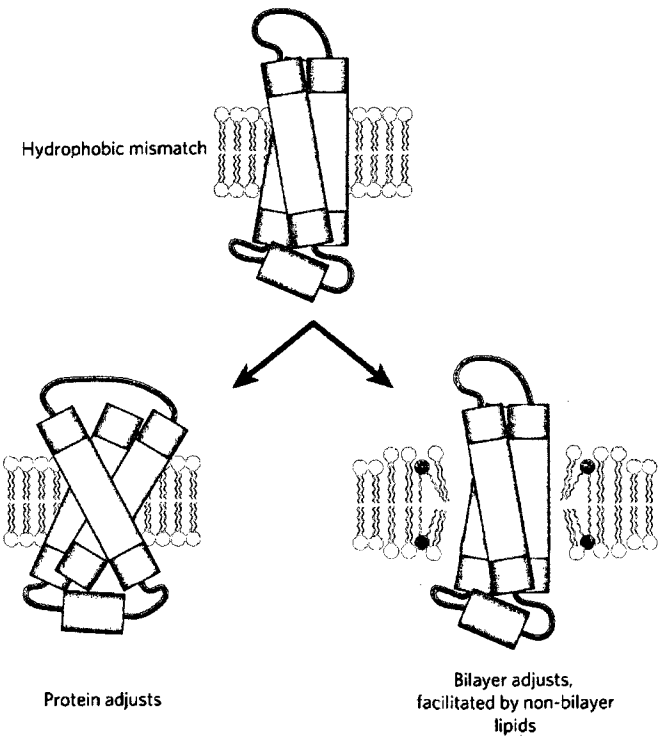

Figure 1.9 Compensation for hydrophobic mismatch from protein. If the hydrophobic length of the protein does not match the hydrophobic chain length of the lipid then the protein can tilt its α-helices to compensate for the hydrophobic mismatch but only up to a certain extent so, protein adjustment cannot compensate solely for hydrophobic mismatch. In natural membranes this mismatch can also be minimized by the other lipid molecules (shown in red) disrupting the lipid bilayer. Figure adapted from [30].

In the case of BRC's, hydrophobic mismatch causes some conformational changes in the protein even if the compensation occurs in the lipid. These conformational changes cause altered rates for the forward electron transfer and/or charge recombination. The charge recombination from primary ($P^+Q_A^-$ ⟶ PQ_A) and secondary quinones ($P^+Q_B^-$⟶ PQ_B) take place in 100 ms and 1 s in the presence of detergent micelles, respectively [23]. The electron transfer is accompanied by proton uptake and conformational changes. After light excitation, the electron travels to the primary quinone (Q_A) and then a further electron

transfer to the secondary quinone (Q_B) depends on the occupancy of the quinone binding site.

The secondary quinone has two different binding sites: proximal and distal as shown in Figure 1.10 [15]. In the distal position, the head group of the quinone is outside of the binding pocket having one hydrogen bond with the protein whereas in the proximal position head group is in the binding pocket with four hydrogen bonds. Reduced quinone (Q_B^-) is always found in the proximal position, consistent with the stabilization of negative charge by the four hydrogen bonds. The electron transfer from primary to secondary quinone is found to be a conformational gating step, where the secondary quinone moves from the distal to the proximal position, which involves a movement of 5 Å and a rotation of the benzene ring along the isoprenoid tail [15]. Similarly, on the periplasmic side, two distinct conformations of the primary electron donor were found depending on the type of detergent micelles in which the BRC's were incorporated [31].

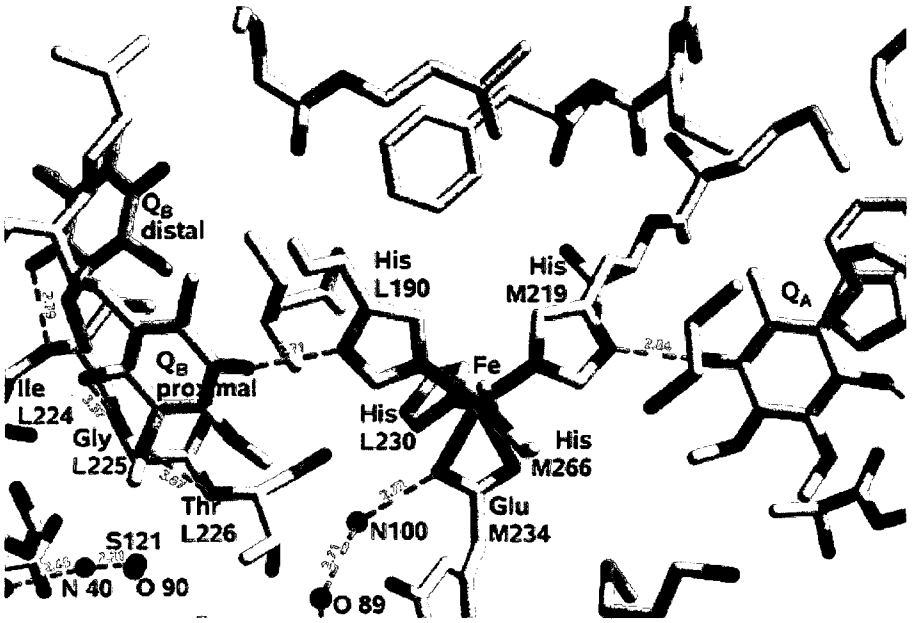

Figure 1.10 View onto the two quinone binding sites of Q_A and Q_B demonstrating the approximate symmetry between Q_A and proximal Q_B position. The central non-heme iron is coordinated by four His residues (L190, L230, M219, and M266) and a Glu residue (M234). Possible hydrogen bonds are indicated by broken green lines, with their length given in Å [32].

Upon continuous, non-saturating illumination, the BRC undergoes conformational rearrangements, which produces altered light adapted conformations with longer lifetimes. The hydrophobic environment (detergent micelles or liposomes) have different effects on these conformational rearrangements, altering the lifetime of the charge separated states. The effect of these hydrophobic environments can be studied along with other parameters like pH, temperature, bound metal ion, effect of detergent concentration, type of detergent, occupancy of quinone binding site etc. on the conformational rearrangements.

1.7 Optical spectrum of *Rb. sphaeroides*

The BRC from *Rb. sphaeroides* can be characterized by optical difference spectroscopy. The absorption spectrum of BRC (Figure 1.11A [33]) shows that in the Q_Y region bacteriochlorophyll dimer absorbs around 865 nm, bacteriochlorophyll monomer absorbs around 800 nm, bacteriopheophytine absorbs around 760 nm and in the Q_X region bacteriochlorophyll absorbs around 600 nm and bacteriopheophytine absorbs around 540 nm. The strong band below 400 nm indicates a Soret band which is characteristic of the porphyrin macrocycle and the aromatic amino acids show absorption around 260 nm [33].

The Q_X and Q_Y are two transition wavelengths, where the Q_X transition has a dipole moment in the direction from ring 4 to ring 2 while the Q_Y has a dipole moment in the direction from ring 3 to ring 1 (Figure 1.11B). Depending on the extent of delocalization, absorption can be observed in different spectral regions. The conjugation level in the direction of the Q_Y transition is more than in Q_X transition therefore the absorption is shifted to longer wavelength. The $(BChl)_2$ has even more conjugation due to the two halves of BChl electronically coupling together, which results in an absorption band of the dimer at 865 nm in the wild type protein.

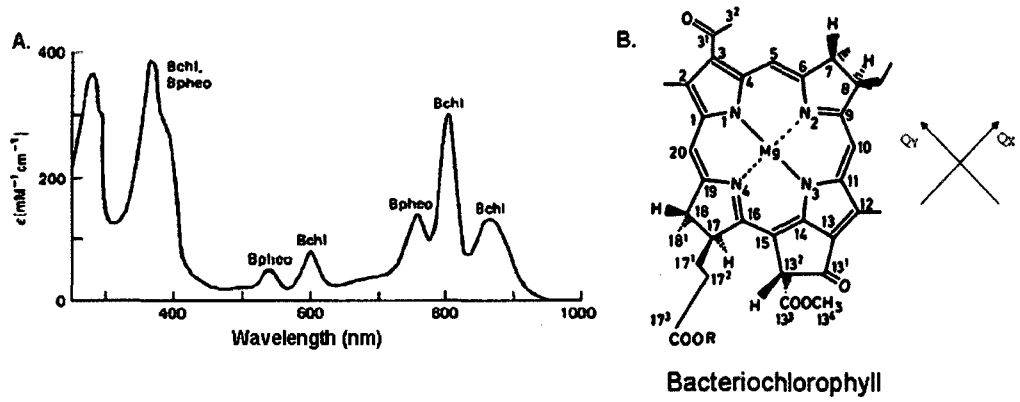

Figure 1.11 Absorption spectrum of the BRC and bacteriochlorophyll molecule. A. Optical spectrum of BRC where the $(BChl)_2$, BChl and Bpheo absorb around 865, 800 and 760 nm in Q_Y transition region respectively while bacteriochlorophylls and Bpheo absorb around 600 and 540 nm in Q_X transition region respectively and **B.** The bacteriochlorophyll molecule, which is a tetrapyrrole system coordinated with central magnesium. R is a phytyl chain. Ring 1 has acetyl and ring 5 has keto carbonyl group. Dipole moments of Q_X and Q_Y transition are from ring 4 to 2 and from ring 3 to 1 respectively. Figure was adapted from reference 33.

The near infrared spectrum is very informative because the bacteriochlorophyll dimer has a strong absorption band at ~865 nm in the dark adapted state of the BRC (Figure 1.12A). During illumination electron transfer takes place from the bacteriochlorophyll dimer and is oxidized resulting in bleaching of the dimer band in the light adapted state *i.e.* BRC which is illuminated (Figure 1.12A).

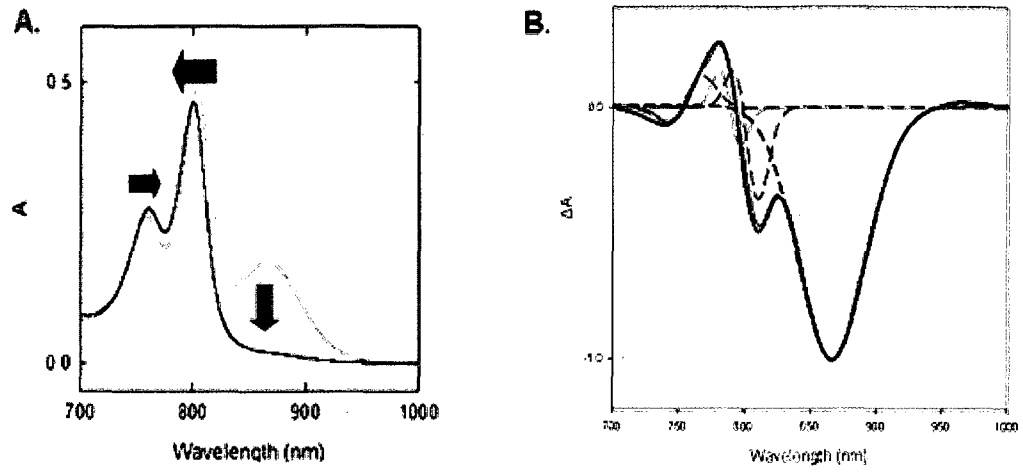

Figure 1.12 NIR light-minus-dark difference spectrum of BRC. A. NIR dark adapted spectrum of BRC is shown in gray. Upon illumination, transmembrane electron transfer takes place from the bacteriochlorophyll dimer to the quinone resulting in the bleaching of the $(Bchl)_2$ dimer band (red arrow), a hypsochromic shift in the Bchl monomer band (blue arrow) and a bathochromic shift in the Bpheo band (dark green arrow). The spectrum recorded under illumination is shown in black. **B.** Light-minus-dark difference spectrum (red trace) can be fit to the sum of Gaussians for $(Bchl)_2$, Bchls and Bpheos to determine the shifts in the band positions from dark adapted to light adapted states. Black trace is the total fit to the measured spectrum. The values of the fit are listed in the text.

The hypsochromic shift in the bacteriochlorophyll monomer band and a bathochromic shift in bacteriopheophytin absorption band in the light adapted state are observed due to electrochromic effects. After taking the difference of these two spectra, small changes in the spectrum can be highlighted (red trace in Figure 1.12B) [23]. Decomposition of the light-minus-dark difference spectrum (Figure 1.12B) reveals the presence of oxidized bacteriochlorophyll dimer (P^+) and the electrochromic shifts in the bacteriochlorophyll monomer and bacteriopheophytine bands. These spectral changes are indicators of the presence of the charge separated state (P^+Q^-).

The light-minus-dark optical spectrum can be decomposed in terms of shifts in the absorption bands of the individual chromophores of the BRC. The ground state spectrum has bands centered at 760, 800, and 865 nm, due to absorption of the bacteriopheophytins, bacteriochlorophyll monomers, and P, respectively (Figure 1.12A) [33]. The widths of the absorption bands were determined by Gaussian fits of the individual bands of the optical spectrum, yielding band widths at half-maxima (BWHM) of 28 nm centered at 865 nm for the P band, 8 nm each centered at 790 and 810 nm for both bacteriochlorophyll monomers contribution to the 800 nm band, and 14 nm centered at 760 nm for both of the bacteriopheophytins. The shift in the bacteriopheophytin band is much smaller and mainly due to the formation of Q_A^-, that band was not decomposed into the two individual contributions for simplicity.

1.8 Kinetic analysis of BRC

Absorption changes at the bacteriochlorophyll dimer band position (865 nm) were monitored for kinetic analysis [47, 57]. Before illumination there was no change in the kinetic trace but after turning on the external illumination source, a sudden change in the kinetic trace was observed due to the instant charge separation ($PQ_A \rightleftharpoons P^+Q_A^-$) (Figure 1.13). After prolonged illumination this charge separated state slowly undergoes into different conformational changes, which can be seen as a slow increase of the signal in the spectral response (note that the absorption changes are negative since the oxidized form of the dimer absorbs the light less

than the reduced form). Once the external illumination is turned off then the charge separated state from the dark adapted state recombines rapidly showing a sudden change in the kinetic trace. The fraction of the charge separated state, which was present in the altered conformation, recovered on a long time scale (Figure 1.13).

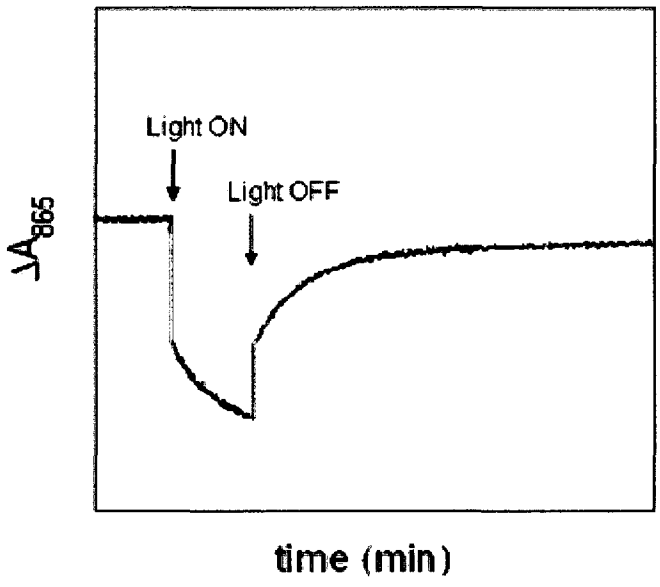

Figure 1.13 Identification of different conformational states formed after the illumination by the kinetic analysis: Multiple components can be distinguished in the kinetic traces. RED component represents sudden change in the absorption upon illumination due to the formation of charge separated state in the dark adapted conformation. Prolonged illumination causes light induced conformational changes resulting in the charge separated state with longer lifetimes. This is shown as the BLUE part of the kinetic trace. The GREEN unresolved part represents the charge recombination from the dark adapted conformation (~100 ms or 1 s from primary or secondary quinone respectively) after turning the illumination OFF, while the PINK part corresponds to the recovery of that fraction of P^+ in reaction centers that are recovering from the light adapted state.

1.9 Research perspective

Life began very early in Earth's history, perhaps 3.5 billion years ago in the form of photosynthetic organism like photosynthetic bacteria and algae [1]. Then oxygen producing photosynthetic bacteria made aerobic life possible on Earth. Nature has created life on Earth in the form of photosynthetic bacteria, which has been present over billions of years, and represents the most efficient biological energy converting system.

The goal of this research project is to identify the conformational changes that take place in the BRC from *Rhodobacter sphaeroides* upon prolonged illumination. The existence of such conformational rearrangements has been known for more than two decades but the explanations from various different studies are by far not unambiguous and still under debate at the molecular level. Since the lifetimes of the redox states are altered significantly by the conformational rearrangements we also set the goal to control and extend the lifetime of the first stable charge separated state in an attempt to demonstrate that the BRC can function as a biocapacitor.

The transmembrane electron transfer creates negative and positive charges separated by a low dielectric medium, the hydrophobic core of the BRC, making it a potential model for a capacitor, provided that the charging and discharging of the capacitor are controlled properly.

First, we will present a study of the conformational changes after systematically altering the local electrostatics and the hydrogen bonding pattern between the

protein and the bacteriochlorophyll dimer, in order to find the cause of the structural changes at the molecular level. Then we demonstrate how to control those conformational rearrangements by systematically changing various parameters like pH, illumination time, temperature, head-group charge of detergent and environment, detergent concentration, presence of a bound metal ion, illumination source etc. With these systematic changes the lifetimes of the charge separated states were increased by 6 orders of magnitude. Part of the research effort presented here is aimed not only for controlling the storage of the electrical potential (increasing the lifetimes) of the proposed biocapacitor but also finding ways to rapidly discharge it.

Chapter 2

Materials and methods

2.1 Growing *Rb. sphaeroides* bacterium

Growth of BRC involves preparation of media, sterilization of media, inoculation and growing bacteria in the presence of light. Growth media was prepared by using 4 g of casamino acid, 4 ml of growth factor, 80 ml of concentrated base, 40 ml of potassium succinate, 80 ml of phosphate buffer (1M), and 25 ml of ammonium sulfate. Finally the volume was adjusted to 4 L.

The growth factor was prepared by combining 2 mg of biotin, 50 mg of sodium bicarbonate, 100 mg of nicotinic acid, 50 mg of thiamine-hydrochloride, and 100 mg of p-amino benzoic acid. The solution was boiled to dissolve all the ingredients and the final volume was adjusted to 100 ml. Once it is dissolved the solution was autoclaved by putting into three smaller vessels.

Concentrated base was prepared by using 12 g of potassium hydroxide and 20 g of nitrilotriacetic acid. The solution was stirred for 20 minutes and only the supernatant was used. Then 58 g of magnesium sulfate heptahydrate, 6.8 g of calcium chloride dehydrate, 200 mg of ferrous sulfate heptahydrate, and 4 ml of ammonium molibdenate solution in the portion of 1 ml were added slowly. All contents were dissolved before adding the next. Finally the 'metals 44' solution was added, pH adjusted to 6.7 and volume brought to 2 L.

'Metals 44' contains 200 mg of EDTA, 1.1 g of zinc sulfate heptahydrate, 500 mg of ferrous iron sulfate heptahydrate, 150 mg of manganous sulfate monohydrate, 40 mg of cupric sulfate pentahydrate, 20 mg cobalt chloride, 12 mg of boric acid, and 150 µl of 6 N sulfuric acid. The volume was adjusted to 100 ml. The color was greenish at the beginning but becomes amber later.

The 20% potassium succinate was prepared by pouring 200 g of succinic acid in a beaker with 250 ml water and stirring, it did not dissolve completely. In another beaker 200 g of potassium hydroxide was dissolved and cooled. Using an ice bath, the potassium hydroxide was added slowly to the beaker containing succinate. The final volume was adjusted to 1 L and pH was brought to 7 by adding HCl.

The 1 M phosphate buffer was prepared by 274 g of dibasic potassium phosphate trihydrate in 1200 ml of distilled water and dissolving 136 g of monobasic potassium phosphate in 800 ml of distilled water then slowly combining the solutions. Final volume was made to 2 L at a pH of 7.

The 10% ammonium sulfate was prepared by dissolving 50 g of ammonium sulfate to 500 ml with pH of 7.

All solutions were prepared in distilled water and final solutions were stored at 4° C.

The growth media was sterilized in an autoclave (type SV-120) scientific prevacuum sterilizer for 1 hour and cooled to room temperature. Inoculation with bacteria was done near the Bunsen burner to avoid any external contamination. The inoculated media was put in the dark for a maximum of 6 hours in order to

consume the oxygen. *Rb. sphaeroides* was grown under anaerobic conditions in the presence of light (60 W power) for two days. Once the cells were completely grown, they were centrifuged using a Beckman J2-HS centrifuge at 4° C at 7,000 g's for 20 minutes with a JA-10 rotor. The supernatant was discarded and all cells were collected and stored at -20° C.

2.2 Purification of BRC

The BRCs were prepared by treatment with the detergent LDAO as described earlier [34-36]. Briefly, 100 g of collected cells were allowed to stir in 200 ml of distilled water and 2 ml of 1 M Tris buffer for 1 hour. At the end of stirring a homogenized solution was obtained. Then 2 ml of EDTA, 1.25 g of sodium chloride salt for ionic strength and 1.7 ml of lauryldimethylamine-oxide (LDAO) detergent was added. The cells were lysed with 40 minutes of sonication in 10 s intervals in a ice bath using a Mandel Scientific company's ultrasound processor to avoid excessive temperature. The final volume of the solution was adjusted to 210 ml, which was filled in 8 tubes and centrifuged at 200,000 g's at 4° C for 2 hours in Beckman Optima XL-100K ultracentrifuge with Ti-70 rotor. After the first centrifugation, pellets were resuspended in 205.34 ml of TEN buffer. TEN buffer contains 15 mM Tris-HCl, 1 mM EDTA, and 0.1 M NaCl. Then 4.66 ml of LDAO was added in the dark and allowed to stir for 10 minutes at room temperature. Centrifugation of this solution was done with same parameters as the above mentioned ultracentrifuge procedure to solubilize BRCs in detergent

micelles. Crude BRC micelles were collected from the supernatant discarding the pellets containing cell membranes. For 220 ml of supernatant 72 g of ammonium sulfate and 7.3 ml of 30% LDAO were used for the isolation of crude BRCs. The mixture was allowed to stir for 15 minutes at room temperature. These crude BRCs were centrifuged at 10,000 g's at 4° C for 15 minutes in Beckman J2-HS centrifuge machine with a rotor type of JA-17 and resuspended in TEN buffer. Resuspended BRC micelles were dialysed overnight dialysis, to remove ammonium sulfate, in $TL^{0.1}E$ which contains 15 mM Tris-HCl, 1 mM EDTA, and 0.1% LDAO.

For further purification of the BRCs, ion exchange column chromatography was used. The Toyopearl 650 M column was equilibrated with $TL^{0.1}E$ buffer then protein was loaded onto the column, which binds to the column material then again $TL^{0.1}E$ buffer was loaded. By creating a linear salt gradient from 0.03 to 0.25 M NaCl in $TL^{0.1}E$ buffer purified protein and other free pigments can be separated. The purity of the BRC protein was checked by taking the ratio of the absorbances at 280 nm and 800 nm. This ratio was kept below 1.5 but for the purest protein this ratio has to be 1.2. Aromatic amino acids have absorbance at 280 nm, which is 1.2 times that of bacteriochlorophyll monomer at 800 nm. For pure BRC, the ratio of absorption bands of bacteriochlorophyll dimer, bacteriochlorophyll monomer and bacteriopheophytine has to be 1:2:1. After the column chromatography, salt was removed by dialysis against salt free $TL^{0.025}E$ buffer, which contained 15 mM of Tris-HCl, 1 mM of EDTA, and 0.025 % LDAO. All dialysis were done at 4° C in the dark using dialysis membranes with

a molecular weight cut off (MWCO) of 12-14 kDa. Bacterial reaction center protein micelles were further concentrated by ultrafiltration using Millipore membranes having a nominal molecular weight limit (NMWL) of 30 kDa under nitrogen pressure. The concentration of BRC protein was checked by absorption ratio spectroscopy. Purified protein was stored at -80° C in the dark. BRC can be incorporated into Triton X-100 detergent micelles by running same column chromatography technique explained before for the purification with $TT^{0.1}E$ (15 mM Tris-HCl, 0.1% Triton X-100 and 1 mM EDTA) buffer and salt gradient was applied to elute protein. All used chemicals were ordered from Sigma-Aldrich.

2.3 Construction of the mutants

A series of reaction center mutants have been constructed by our collaborators to modify the hydrogen bonding pattern on the conjugated carbonyl groups of P by introducing histidine residues in the hydrogen bonding position or replacing His L168. In the mutants, Leu to His at L131, LH(L131), Leu to His at M160, LH(M160), Phe to His at M197, FH(M197) and His to Phe at L168, HF(L168), the formation and removal of hydrogen bonds were confirmed both by Raman and infrared spectroscopies [37-42]. Comparison of reaction centers with different combinations of hydrogen bonds in terms of the light-minus-dark optical difference spectra and the kinetics of the absorbance changes after long continuous illumination allowed us to identify the contribution of hydrogen bonds to possible structural changes involving P.

The construction of the mutant strains of *Rb. sphaeroides* by oligonucleotide-directed mutagenesis has been described before [29-31] and construction was done by our collaborators. The term wild type used in this study refers to those isolated from the deletion strain complemented with a plasmid bearing the wild-type reaction center genes. Reaction centers were kept in 15mM Tris-HCl, pH 8.0, 0.025% LDAO and 1 mM EDTA. The purity of the reaction centers, defined as the ratio of the absorbance at 280 nm to 802 nm, was between 1.2 and 1.4 for all preparations used in this study.

Terbutryn (100 μM) in ethanol was used as an inhibitor, which binds competitively to the secondary quinone binding site, preventing further electron transfer.

2.4 Buffer preparation

Different buffers were used for different pH and different detergent micelles. These buffers were prepared in distilled water by taking 15 mM of respective buffer, 0.1 % LDAO (zwitterionic) or Triton X-100 (non-ionic) detergent, and 1 mM EDTA. The following buffers were used for different pH measurements.

pH 5.5: MES (2-(*N*-morpholino)ethanesulfonic acid)

pH 6: MES (2-(*N*-morpholino)ethanesulfonic acid)

pH 7: BIS-TRIS Propane (1,3-bis(tris(hydroxymethyl)methylamino)propane)

pH 8: BIS-TRIS Propane (1,3-bis(tris(hydroxymethyl)methylamino)propane)

pH 9: CHES (*N*-Cyclohexyl-2-aminoethanesulfonic acid)

pH 10: CAPS (*N*-cyclohexyl-3-aminopropanesulfonic acid)

2.5 Biophysical techniques used in the characterization

2.5.1 Laser flash photolysis (LFP)

To measure the kinetics of the charge recombination reactions, a laser flash photolysis unit (LFP-112) with a Nd:YAG laser from Luzchem Research Incorporation's (Ottawa, Canada) was used. The BRC protein was excited at 532 nm with a 5 ns saturating laser pulse directed perpendicularly to the direction of the monitoring beam and data were collected by monitoring the transient absorption changes at 865 nm. The monitoring light was generated by an "ozone-free" Xe lamp and was guided to the sample with fiber optics. For better signal to noise ratio, 10 traces were averaged with manual laser fire. All data were collected on a Tektronix TDS-2012 oscilloscope in DC coupled mode, which was used as an analog to digital converter. The digitized signal was then processed using a software supplied with the LFP unit. The recorded traces were analyzed with Sigma Plot software by decomposing the signals to exponentials. Bacterial reaction center protein (1 μM) was added in 3 ml of respective buffer with 100 μM terbutryn to block the secondary quinone binding site and charge recombination was measured by recording the kinetic trace at dimer band position (865 nm) in a 3 ml quartz cuvette.

2.5.2 Steady state absorption spectroscopy

All measurements for conformational rearrangement and charge recombinations were measured with a Varian (Varian Inc. Mulgrave, Victoria, Australia) spectrophotometer or a Cary 5000 UV-VIS-NIR. An external tungsten lamp light

source with output power of 40 to 250 W was connected to the cuvette holder by using an optical fiber to illuminate the BRC sample.

The light-induced states of the reaction centers were generated by continuous illumination through the tungsten lamp and its intensity was altered by changing the power of the illumination source. The light intensity was set to ~30% of the saturating value for wild type at a 2 μM reaction center concentration. Terbutryn was used at a concentration of 100 μM to eliminate secondary quinone activity. The measurements were taken in the 3 ml quartz cuvette with the following parameters.

Scanning wavelength: 700-1000 nm

Average time to scan: 0.033 s

Data interval: 0.5 nm

Scan rate: 909.091 nm/min

Spectral bandwidth: 2 nm

The light-minus-dark difference spectra were recorded by taking baseline with the BRC sample and then a series of spectra were recorded during and after the prolonged illumination with 1 minute intervals up to 5 minutes and with 5 minute intervals until the signals recovered completely. During illumination the spectra were recorded every minute.

For the temperature-dependent measurements, a dual Peltier-cell accessory was connected to the cuvette holder and the temperature was varied from 5 to 40° C with 0.1° C accuracy including water circulation around the Peltier-cell for cooling.

Matching buffers were used as the reference and the baseline was recorded prior to each measurement. Kinetic analysis was done in kinetic mode of the spectrophotometer by monitoring the absorption change at 865 nm *i.e.* bacteriochlorophyll dimer band position.

For the metal binding study to BRC, Co^{2+}, Mn^{2+}, and Cu^{2+} metal ions were titrated in BRC sample in the cuvette and kinetic traces were recorded at different concentrations of metal ion with 5 minutes of illumination.

To change the pH during the measurement, the lid of the spectrophotometer was kept open by deactivating the sensor switch for the lid. After turning off the illumination, while continuing the measurement, the pH was increased from 6 to 10 by addition of potassium hydroxide solution and the kinetic trace was recorded. A small magnetic stirrer was used to mix the solution in the cuvette which was controlled by Peltier cell assembly.

2.6 Data analysis

2.6.1 Analysis of the kinetic traces

Kinetic traces of the charge recombination were measured by LFP and absorption spectroscopy depending on the time scales characteristic to the various conformational substates. This charge recombination was analyzed by exponential decomposition assuming three kinetic componets according to following equation:

$$A(t) = Be^{-k_1 \times t} + Ce^{-k_2 \times t} + De^{-k_3 \times t} \qquad (1)$$

Where,

A: total signal amplitude at any time t

B, C, and D: amplitudes of the decaying kinetic components

t: time

k_1, k_2, and k_3: Rate constants of the decaying kinetic components

Standard errors in determining the rate constants on the fitted data are within $\pm 0.5\ s^{-1}$.

$$\text{Time constant } (\tau) = \frac{1}{k} \qquad (2)$$

Where, k is the rate constant of the kinetic component.

The temperature dependence of charge recombination was analyzed by using the Arrhenius equation:

$$\ln(k) = \frac{-E_a}{RT} + \ln(C) \qquad (3)$$

Where,

k: first order rate constant of the charge recombination

E_a: activation energy

R: universal gas constant

T: absolute temperature

C: maximal electron transfer rate constant in the activationless process

In an Arrhenius plot, ln(k) versus $\frac{1}{T}$ gives a straight line and it's slope can be used to determine the activation energy (E_a).

2.6.2 Analysis of metal binding

The Hill equation was used to fit the data of metal binding.

$$k = \frac{[M]^{n_H}}{K^{n_H} + [M]^{n_H}} \tag{4}$$

Where,

k: rate constant of decaying component

K: binding constant

n_H: Hill constant

[M]: metal ion concentration

2.6.3 Decomposing the absorption spectra into individual components

Fitting of the ground state spectrum was done by sum of Gaussians for the bacteriochlorophyll dimer, bacteriochlorophyll monomer, and bacteriopheophytin as follws:

$$A = C + a \times e^{-0.5 \times (\frac{W - W_0}{L})^2} \tag{5}$$

Where,

A: absorbance at any given wavelength

C: offset, applied if the traces did not recover to zero

a: peak absorbance

W: wavelength

W_0: peak position in the wavelength scale

L: Bandwidth at half maxima (BWHM)

2.6.4 Determining the proton dissociation constant

The Henderson-Hasselbalch curve was used to explain pK shifts of the amino acid residues, which is expressed by the following equation:

$$f(H) = \frac{1}{1+10^{(pH-pK)}} \quad (6)$$

Where,

f(H): fraction protonated

pK: negative logarithm value of the proton dissociation coefficient

Experimental Results

Chapter 3

Molecular assignments of the conformational rearrangements based on genetic modifications near the periplasmic side of the BRC's

3.1 The formation and disappearance of the conformationally altered charge separated states upon prolonged illumination in the wild type BRC's

Light-minus-dark difference spectra were recorded during and after prolonged illumination of the BRC samples. These spectra were analyzed for spectral band shifts. Representative light-minus-dark spectra are shown below in Figure 3.1 They were decomposed into the following contributions a bleaching in the $(BChl)_2$ band (865 nm), shifts in the two BChl (790 and 810 nm) and in Bpheo bands (760 nm) for analysis purposes as described earlier in Section 1.7.

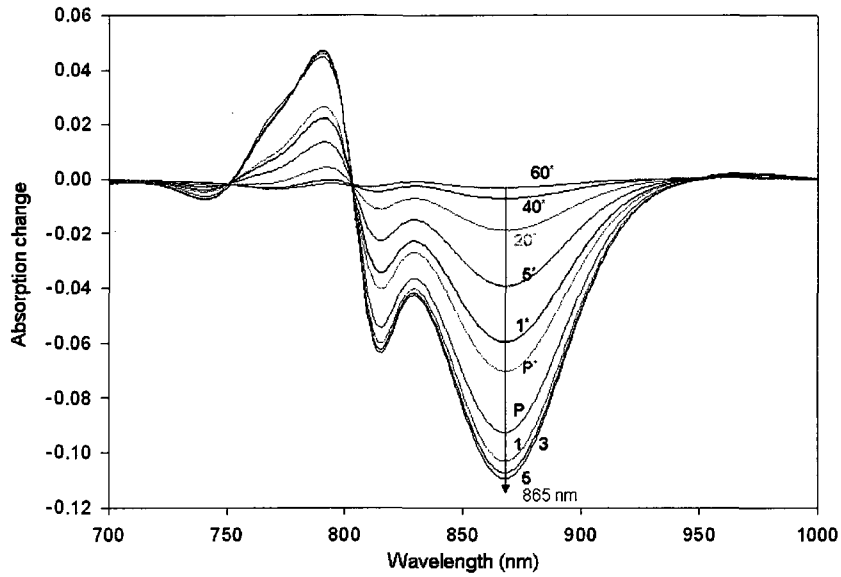

Figure 3.1 Representative near infrared light-minus-dark difference spectra. Steady state absorption difference spectra reveal the features from the oxidized $(BChl)_2$ at 865 nm, the hypsochromic shift in BChl and bathochromic shift in Bpheo bands. Light-minus-dark difference spectra were recorded immediately after illumination (P) untill 5 minutes of illumination. The color code of the spectrum and number represent time in minutes after the illumination turned ON. The P^* spectrum was taken immediately after illumination turned OFF. The numbers with prime indicate the time in minutes after illumination was turned OFF. Conditions: Spectra were recorded from 1 μM of wild type BRC in 0.1% LDAO detergent at pH 8 with 100 μM terbutryn upon 5 min of illumination. The tungsten lamp (120 W) was used as illumination source.

Each of the recorded spectrum had spectral signatures of the charge separated state P^+Q^- revealing the formation of the charge separated state upon illumination but with an altered lifetime. In order to study the kinetics of recovery of the oxidized bacteriochlorophyll dimer, absorption changes were monitored at the dimer band position 865 nm indicated by the vertical line in the Figure 3.1 The series of the kinetic traces were recorded at the dimer band position by varying illumination time from 5 s to 10 minutes (Figure 3.2). The representative kinetic

traces for different illumination times show multi-exponential recovery of oxidized bacteriochlorophyll dimer monitored at 865 nm. For the very short illumination of 5 s (red trace in the Figure 3.2), the recovering component is only bi-exponential. The fast kinetic component is attributed to the charge recombination from the dark adapted conformation and the slower component is assigned to the charge recombination from an altered conformation caused by the prolonged illumination. With increasing illumination time a slow evolution of longer lived components could be observed (Figure 3.2).

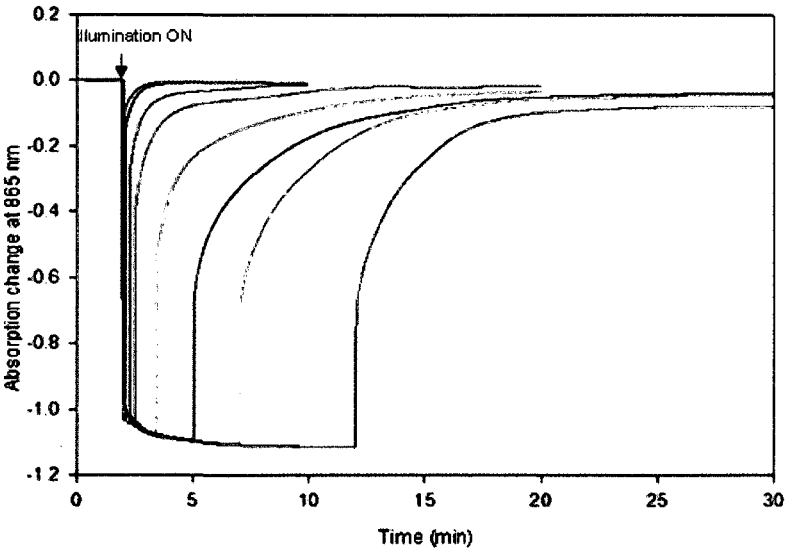

Figure 3.2 Representative normalized kinetic traces for the formation and disappearance of the long lived charge separated states upon increasing illumination time monitored at the dimer band position (865 nm in wild type). Traces were recorded after 5s (red), 10 s (dark blue), 30 s (green), 1 min (pink), 2 mins (cyan), 3 mins (gray), 5 mins (mustard), and 10 mins (brown) of illuminations. The recovery kinetics become multiphasic requiring up to three kinetic components to describe them. The traces were fit to Equation (1) and the results of the fits are tabulated in Table 3.1. Conditions: Traces were recorded containing 1μM of wild type BRC in 0.1% LDAO detergent with 100 μM terbutryn at pH 8 with varying illumination time from 5 s to 10 minutes with a tungsten lamp (120 W).

Table 3.1 Kinetic parameters of the wild type reaction center upon 5 s to 10 minutes of prolonged illumination.

Time (s)	[a]k_{slow} x 10^2 (s^{-1})	[b]$k_{slowest}$ x 10^3 (s^{-1})
5	4.7	[c]ND
10	4.6	[c]ND
30	4.6	5.2
60	2.8	5.2
120	2.8	5.1
180	2.6	3.3
300	2.5	2.4
600	2.5	2.4

[a]Rate constants of the slow recovering component (determined from Figure 3.2);
[b]Rate constants of the slowest recovering component (determined from Figure 3.2);
[c]ND- not detectable

Upon prolonged illumination, same P^+Q^- charge separated states can be formed (Figure 3.1) but with increased lifetimes and hence they were attributed to the altered conformational states (Figure 3.2). The rate constants of slow and the slowest components in the recovery kinetics were found to be in the 10^{-2} s^{-1} and around 10^{-3} s^{-1} ranges, respectively (Figure 3.2). These two slow kinetic components are missing from the charge recombination induced by a single laser flash excitation and therefore were assigned to the recovery of the charge pair from different conformational states. The charge recombination from the dark

adapted state has a rate constant in the wild type of 10 s^{-1} or 1 s^{-1} depending on presence or absence of the potent inhibitor terbutryn, respectively. Based on the kinetic separation of the components, proposals for conformational changes in the reaction center stem primarily from the observation of multiphasic kinetics in the light-induced absorption changes.

There is also another way to look for these conformational changes. The light-minus-dark difference spectrum was recorded immediately after illumination and after prolonged illumination of 2 minutes in the wild type BRC (Figure 3.3A). The difference between these two spectra should indicate the altered conformation due to the prolonged illumination. The wild type BRC has a carotenoid pigment near $BChl_B$ (Figure 3.3C). It was also found that during illumination the BChl bands in the wild type BRC underwent spectral band shifts (Figure 3.3B). Analysis of the light-minus-dark spectrum revealed that immediately after illumination the $BChl_A$ band moved hypsochromically from 786 to 783 nm. Further illumination caused a reversing red shift to 785 nm. In summary, initial illumination causes a blue shift in the $BChl_A$ and prolonged illumination reverses this shift. The $BChl_B$ undergoes similar shifts from 810 nm to 802 nm and further reversing red shift to 805 nm. The difference between the two light-minus-dark spectra revealed a major change in the BChl band around 800 nm (red trace in Figure 3.3B). This altered conformation has individual contributions from the $BChl_A$ and $BChl_B$.

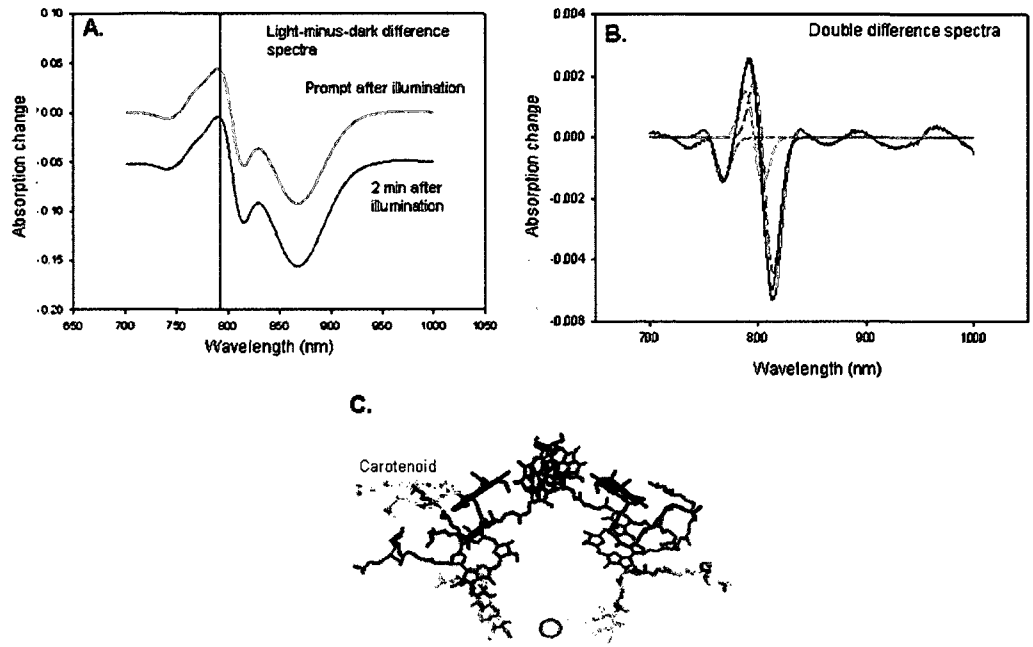

Figure 3.3 Light-minus-dark difference spectra for recovery of the P^+Q^- state in the wild type BRC. A. Light-minus-dark difference spectra, immediately after (red trace) and 2 min (black trace) after the illumination. The spectrum recorded after 2 min of illumination represents the P^+Q^- redox state in an altered conformation. The spectra are vertically shifted by 0.05 AU for better comparison. During recovery from these states, BChl bands were found to be shifted that indicated altered long lived conformational states. **B.** Double difference spectrum (red trace) generated from the difference between prompt and 2 min after the illumination represents the altered conformation at the monomer band ~ 800 nm. Black trace represents total fit. $BChl_B$ (dotted pink trace) shifted from 805 to 802 nm, $BChl_A$ (dotted cyan trace) moved from 785 to 783 nm, and Bpheo (dotted green trace) shifted from 755 to 751 nm during this conformational rearrangement. **C.** The wild type BRC with carotenoid pigment (beige colored molecule) near $BChl_B$. Figure was prepared by Pymol software from PDB code 1M3X. Conditions: 1 μM of BRC micelles from the wild type reaction center in 0.1% LDAO detergent with 100 μM terbutryn at pH-8 with 2 minutes of illumination using a tungsten lamp (120 W).

3.2 Spectral signatures of the conformationally altered states in the R-26 mutant

A similar shift for the bacteriochlorophyll monomer was observed in the case of mutant (R-26), which differs only from wild type by the lack of a carotenoid molecule near the $BChl_B$ (Figure 3.4C). The double difference spectrum (Figure 3.4B) showed that in this strain of the BRC, the shift in the bacteriochlorophyll dimer band was also observed along with the $BChl_A$.

Clues to the conformational arrangements in the vicinity of the dimer can be found in the optical spectra, where upon illumination changes in the BChl bands are observed in the wild type BRC (Figure 3.3B). These changes lead to the longer lifetimes of the same charge separated states. This argument was supported by the similar shifts in the BChl bands in the carotenoidless strain R-26 (Figure 3.4B).

Much of this spectroscopic work was centered on the quinones. Light-induced structural changes of the quinones were indicated by significant differences in the rate of $P^+Q_A^- \rightarrow PQ_A$ charge recombination for reaction centers cooled under illumination compared to cooled in the dark [32, 43]. Two, or more, phases observed in the $Q_A^- \rightarrow Q_B$ electron transfer have been interpreted by assuming a conformational gating mechanism [44-46].

In contrast to the detailed information concerning the conformational changes involving the quinones, no specific structural changes involving the tetrapyrroles or specific amino acid residues have been identified [47].

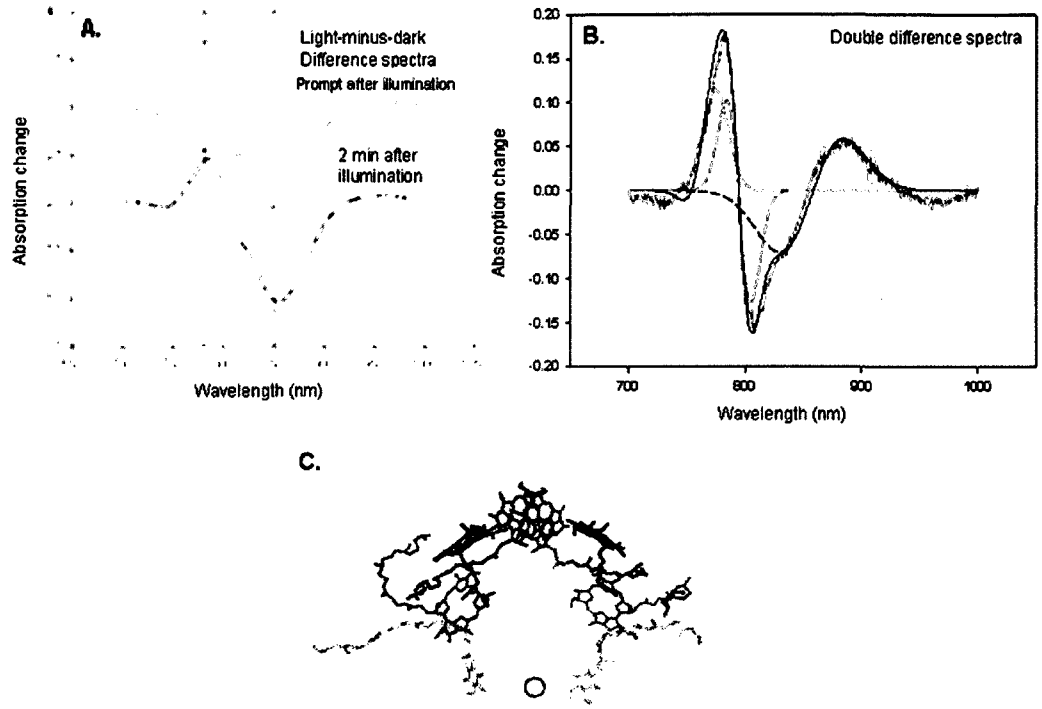

Figure 3.4 Light-minus-dark difference spectra for recovery of P^+Q^- state in the R-26 BRC mutant A. The light-minus-dark difference spectra were recorded in LDAO at pH 6 immediately and 2 min after illumination. The spectra are vertically shifted by 1 AU for better comparison. During recovery from these states the BChl monomer and dimer bands were found to be shifted which caused altered long lived conformational states. **B.** Double difference spectrum (in red) was generated by subtracting the light-minus-dark difference spectra. The black trace is the total fit to the spectrum. It reveals the major change in $BChl_A$ (pink) from 796.5 to 794.5 nm, change in $(BChl)_2$ (purple) from 850.5 to 853.5 nm, which indicates the movement of the bacteriochlorophyll dimer with respect to the bacteriochlorophyll monomer and Bpheo (green). There was a 3 nm red and 2 nm blue shift found in $(BChl)_2$ and $BChl_A$ respectively. Similarly, it shows prolonged illumination causes an initial blue shift in the $BChl_A$ and subsequent red shift. **C.** The R-26 BRC that lacks carotenoid pigment near the $BChl_B$. The figure was prepared by Pymol software from PDB code: 4RCR. Conditions: 1 μM of BRC from carotenoidless R-26 strain in 0.1% LDAO detergent with 100 μM terbutryn at pH-8 with 5 minutes of illumination using tungsten lamp (120 W).

3.3. Light-induced conformational changes in mutants with altered hydrogen bonding pattern between the dimer and the surrounding protein

A number of specific interactions of the amino acid residues with the dimer have been investigated. The two bacteriochlorophylls of P contain two π-conjugated groups, the 2-acetyl and the 9-keto carbonyl, that are possible proton acceptors for hydrogen bonds.

Structural and spectroscopic data demonstrate that in the wild-type *Rb. sphaeroides* reaction center only one hydrogen bond exists between His L168 and the 2-acetyl group of the L half of the dimer [37] (Figure 3.5A). In order to identify the conformational changes at the molecular level a series of reaction center mutants have been constructed by our collaborators to modify the hydrogen bonding pattern on the conjugated carbonyl groups of P by introducing histidine residues in the hydrogen bonding position or replacing His L168 (Figure 3.5B).

The light-minus-dark difference spectra in the near infra-red region for the BRCs representing all four hydrogen bonds between the dimer and the surrounding amino acids (triple mutant-[LH(L131)+LH(M160)+FH(M197)]) and the wild type were recorded (Figure 3.5C). The spectrum of the triple mutant showed a marked blue shift at around 790 nm involving the bacteriochlorophyll monomer compared to the spectrum of the wild type. The double difference spectrum was generated by taking the difference between the light-minus-dark difference spectra of the wild type and triple mutant showed a marked blue shift in the bacteriochlorophyll monomer band (red trace in Figure 3.5D).

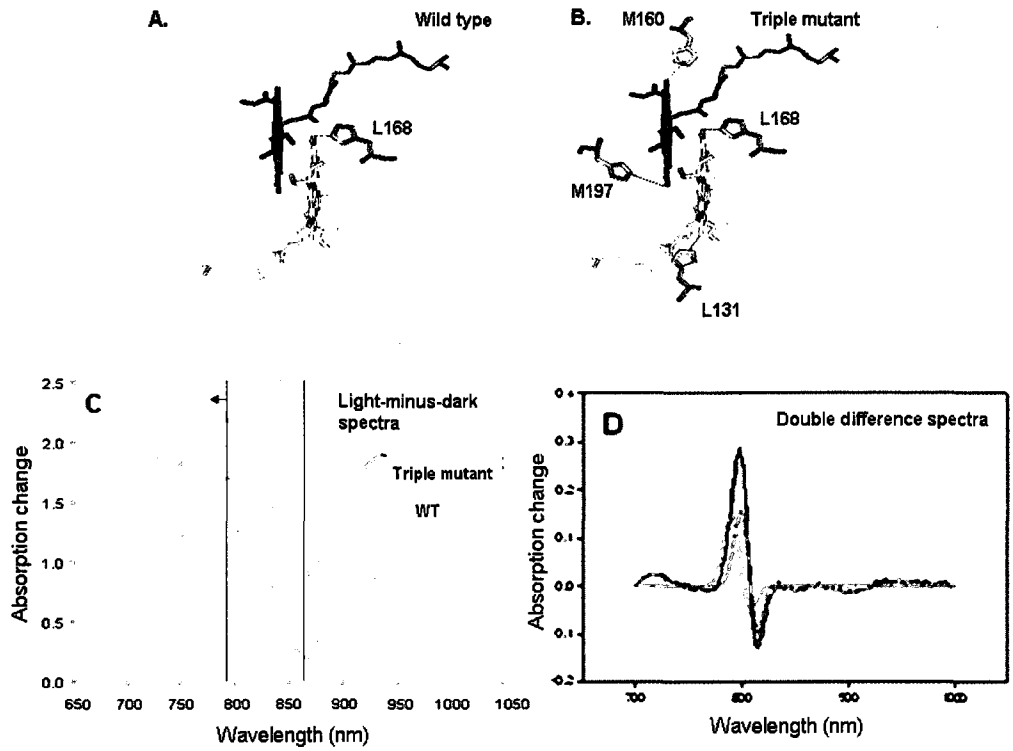

Figure 3.5 Comparison of the light-minus-dark difference spectra for the wild type and triple mutant BRC. Top view of the bacteriochlorophyll dimer (upper panel). **A.** L half of the dimer (yellow) has one hydrogen bond (green dotted line) to His (LH-168 in orange) in wild type reaction center. **B.** Bacteriochlorophyll dimer and nearby amino acid residues. The mutant dimer has four hydrogen bonds (green dotted lines) to the His residues (orange) created by mutations. **C.** The light-minus-dark difference spectra recorded for both the wild type (WT) and mutant RCs, which indicates the shift in the bands of the BChls towards the blue from 790 nm to 784 nm in the triple mutant compared to the wild type. The spectra are vertically shifted by a constant offset. **D.** The double difference spectrum (in red) revealing the major change that was fitted (black trace) with Gaussians involving $BChl_A$ (cyan) and $BChl_B$ (pink). The fit shows that $BChl_B$ moved from 811 to 803 nm and 6 nm blue shift in $BChl_A$ band from 790 to 784 nm. The structure figures were prepared by Pymol software by using PDB files 1Z9J and 4RCR for the mutant and wild type reaction centers respectively. Conditions: 2 μM reaction center at pH 8, 100 mM NaCl, 100 μM terbutryn. Illumination time: 1 minute through a 870 nm interference filter with a bandwidth of 20 nm using water bath as a heat filter between the illumination source and the BRC sample.

After comparing light-minus-dark spectra of the wild type and the triple mutant, it was found that there was only change in the bacteriochlorophyll monomer (Figure 3.5), which was shifted towards blue region in case of the triple mutant [47]. There was no change in the bacteriochlorophyll dimer because in the triple mutant the bacteriochlorophyll dimer was immobilized. Hence upon illumination it cannot undergo any movement but movement of the monomers cannot be prevented.

In case of BRC's from the carotenoidless R-26 strain the bacteriochlorophyll dimer can undergo movement with respect to the bacteriochlorophyll monomer due to the permanent dipole and induced dipole attractive force (Figure 3.4), which causes formation of long lived conformational states. In the triple mutant the bacteriochlorophyll dimer was fixed by hydrogen bonds, and it cannot undergo any movement with respect to the bacteriochlorophyll monomer and hence cannot form long lived conformational states (Figure 3.5).

Since the spectral bandshift associated with the accessory bacteriochlorophylls ($BChl_A$ and $BChl_B$) are due to dipole-dipole interactions from these two experiments we concluded that during prolonged illumination these pigments moved from the dimer and changed the distances and/or the angles between the dipoles as evidenced by change in the electrochromic shifts.

The light-minus-dark optical difference spectra of the mutants

In order to investigate the contribution from each of the hydrogen bonds to the bacteriochlorophyll dimer, a systematic study of the mutants altering the amino acid environment near the dimer was carried out. Therefore for further investigation of the light-induced conformational changes, light-minus-dark difference spectra in the near infrared region were measured for the reaction centers from the wild type and the 11 hydrogen-bonding mutants with different hydrogen bonding pattern (Figure 3.6). Significant differences were found in the position of the Q_Y band of the dimer, which is at 865 nm in the wild type, as reported earlier for absorption spectra of the mutants [41]. Generally, the formation of a hydrogen bond on the M half of the dimer resulted in a blue-shift in the position of the dimer band and the addition of the L half one caused a red-shift in this parameter. The presence of the hydrogen bond between the 2-acetyl group of the L half of the dimer and the histidine at the L168 position in the wild-type reaction centers results in a 16 nm red-shift relative to the HF(L168) mutant (His residue was replaced to Phe at L168), which lacks any of the hydrogen bonds. Interestingly, the introduction of the symmetrical hydrogen bond between the 2-acetyl group of the M half of the dimer and the histidine substituted at the M197 position resulted in a shift of almost the same magnitude (- 17 nm) but in the opposite direction (to the red) in the HF(L168)+FH(M197) double mutant with respect to the hydrogen-bond-less HF(L168) mutant. Formation of the hydrogen bonds with the 9-keto groups on both sides of the dimer showed smaller shifts of - 9 nm (to the blue) and + 7 nm (to the red) in the HF(L168)+LH(M160)

and HF(L168)+LH(L131) double mutants, respectively, relative to the HF(L168) mutant. The differences in the position of this band were smaller in mutants with more than one hydrogen bond. For example, the shift resulting from the second hydrogen bond to the M-side is only - 2 to - 3 nm in the LH(M160) and FH(M197) mutants relative to the wild type, which has one hydrogen bond. A small shift of + 5 nm was also observed for the presence of the hydrogen bond to the L side of the dimer in the LH(L131) mutant. At the level of three and four hydrogen bonds the observed shifts become negligible [47].

The near infrared $P^+Q_A^-/PQ_A$ optical difference spectra of the mutants showed differences in the position of the Q_Y band of the dimer and in the position of the peak centered to 790 nm in wild type (Figure 3.6). Generally, the keto-groups caused smaller changes in the position of the dimer band compared to the acetyl groups.

Changes were also seen in the near-infrared absorption band of the accessory bacteriochlorophyll, which upon light excitation undergoes an electrochromic shift due to the oxidized dimer. The basis of the comparison was the position of the peak observed around 790 nm in the wild-type spectrum (Figure 3.6) corresponding to the $BChl_A$. Those mutants that contain the LH(L131) mutation showed a significant (- 6 to - 9 nm) blue shift in the position of this peak relative to the wild type, while the other mutants resulted in no or negligible (- 1 to - 2 nm) changes (Figure 3.7). A consistent difference for the reaction centers containing the LH(L131) mutation was in the position of the lower wavelength

band (790 nm in wild type) of the electrochromic shift on the accessory BChl (Figure 3.6).

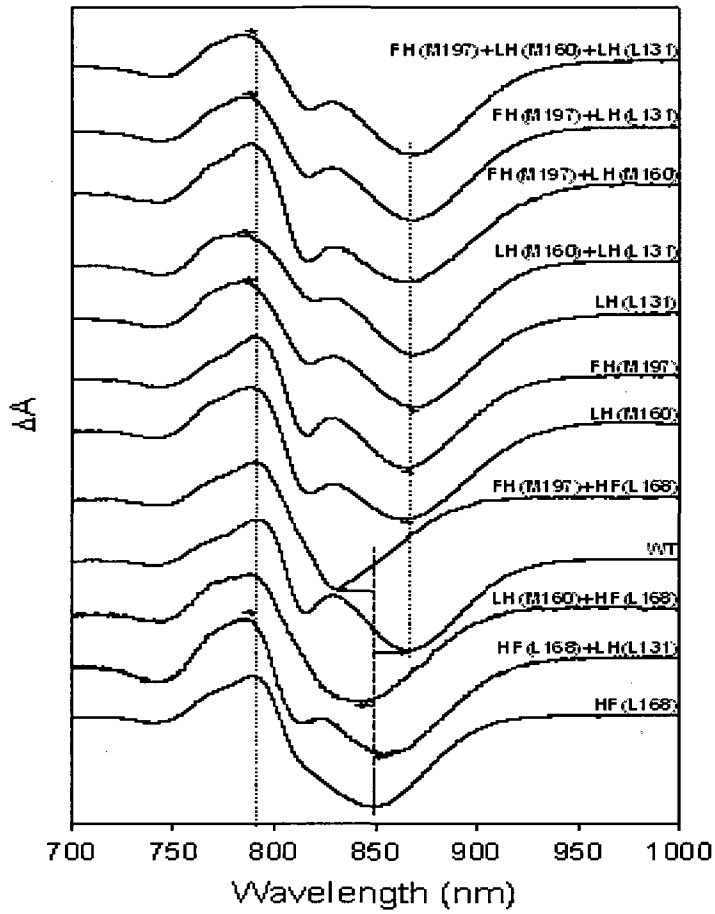

Figure 3.6 Near infrared light-minus-dark absorption difference spectra of reaction centers isolated from the wild type (WT) and hydrogen bond mutants of *Rb. sphaeroides*. The spectra were taken using nonsaturating (30% of the saturating value for wild type) continuous illumination. The spectra are normalized to the Q_Y band of the dimer (832-870 nm depending on the mutant) and vertically shifted by a constant offset for better comparison. Peak positions are tabulated in Table 3.2. Conditions were as follows: 2 μM reaction centers in 15 mM Tris (pH 8), 0.1% LDAO, 1 mM EDTA, 100 mM NaCl, and 100 μM terbutryn. Illumination time: 1 minute through a 870 nm interference filter using water bath as a heat filter [47].

Since the electrochromic shift on the BChl originates from the interaction between the permanent dipoles of P^+ and the induced dipoles of BChl, this reflects either different orientations of the permanent dipoles of P^+ in the mutants or interactions between the altered residue and the bacteriochlorophyll monomer.

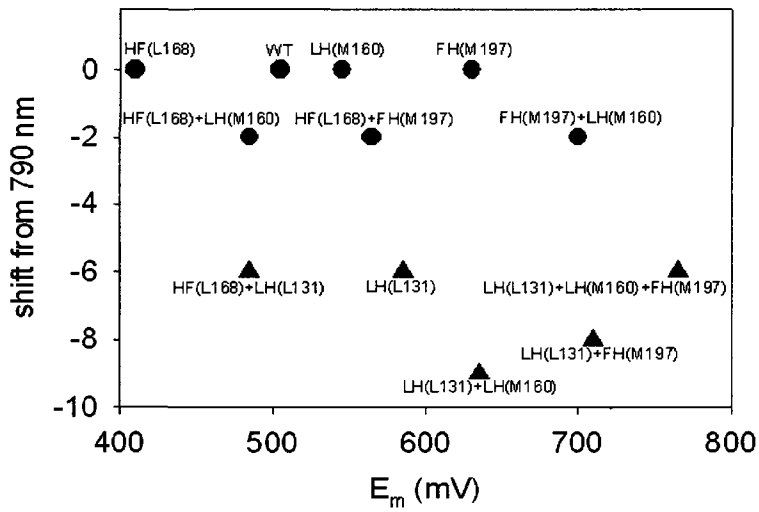

Figure 3.7 Shift in the $BChl_A$ in the mutants against oxidation potential of the dimer from respective mutant with respect to the wild type reaction center. In wild type BRC, $BChl_A$ absorbs at 790 nm. In LH(L131) mutants $BChl_A$ shifts towards blue by 6 to 9 nm (triangles) while the other family of the mutants show only 1 to 2 nm shift as compared to wild type BRC. The oxidation potentials (E_m) of the mutants were determined earlier [41].

Due to these pronounced shifts in the $BChl_A$ in the case of mutants having LH(L131) hydrogen bond with respect to the wild type BRC, these different mutants were categorized into two families, the mutants which do not have LH(L131) hydrogen bond and mutants which have LH(L131) hydrogen bond. After studying the effect of presence of different hydrogen bond to the dimer,

absorption changes were monitored at the respective dimer band position of the mutants (Figure 3.6) for the kinetic study of recovery of the oxidized dimer.

Kinetics of the formation and recovery of the light-induced states in the mutants

The kinetics of the absorption changes caused by non-saturating illumination were measured at the center of the Q_Y band of the dimer observed in the reaction centers from each mutant (Figure 3.8) at pH 8. In the presence of terbutryn, the $P^+Q_A^-$ state is formed within a few tens of milliseconds, but electron transfer to the secondary quinone is inhibited. In addition to the rapid absorption change, a further slower bleaching was also observed in all reaction centers. Since the excitation was non-saturating, with only ~30% of wild-type reaction centers excited, this increase in kinetic trace can be interpreted as arising from another light-induced state being formed with a longer lifetime. Once the light is turned off, complex recovery kinetics were observed that depended on the duration of the illumination, and the mutation (Table 3.2). A one minute illumination was used at pH 8 to compare the recovery kinetics of the oxidized dimer. A fraction of the reaction centers followed the fast $P^+Q_A^- \rightarrow PQ_A$ charge recombination while the rest of the oxidized dimer recovered on a much longer time scale.

In reaction center mutants containing the Leu to His mutation at L131, the slower component of the P^+ decay was 7 to 8 s, corresponding to rate constants of 12 to 14 x 10^{-2} s^{-1}. In reaction centers without this mutation, this kinetic parameter was longer, with lifetimes of 30 to 63 s, corresponding to rate constants of 1.6 to 3.3 x 10^{-2} s^{-1}. The LH(M160)+FH(M197) mutant showed an intermediate value

with a 14 s lifetime, or a k_{slow} of 7.1 x 10^{-2} s^{-1}, for that slow phase. The relative contribution of the slow phase in the formation (during the illumination) and in the recovery (in dark) is much smaller in the case of the LH(L131)-containing mutants and the LH(M160)+FH(M197) double mutant compared to the others (Figure 3.8 and Table 3.2).

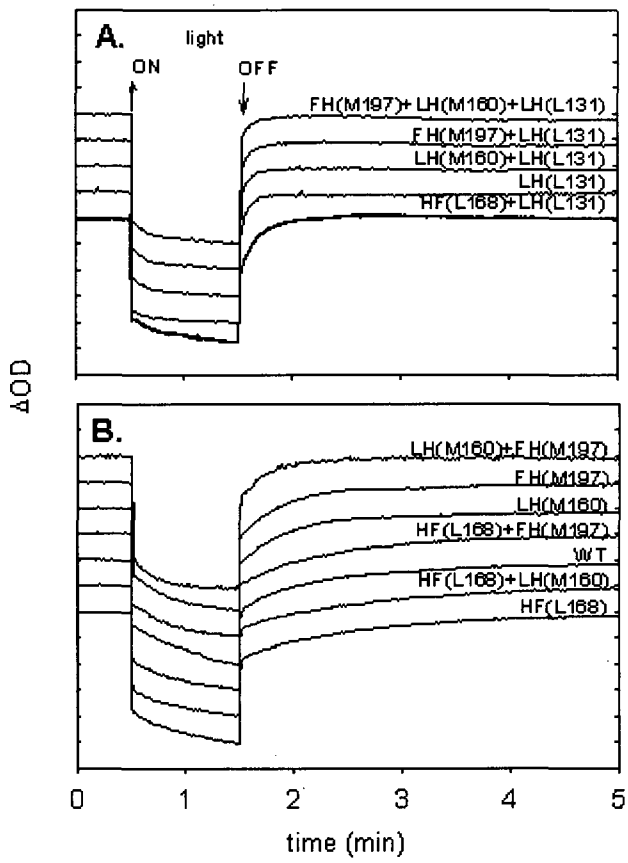

Figure 3.8 Formation and disappearance of the continuous light induced $P^+Q_A^-$ state in the wild type and 11 hydrogen bonding mutants measured at the position of the dimer band (832-870 nm depending on the mutant, see Figure 3.6) at pH 8. A. Mutants containing the LH(L131) mutation. **B.** All other mutants and wild type. Illumination time is 1 minute. The traces were normalized to 1 and vertically shifted for better comparison. Conditions were as follows: 2 μM reaction centers in 15 mM Tris (pH 8), 0.1% LDAO, 1 mM EDTA, 100 mM NaCl, and 100 μM terbutryn. Illumination time: 1 minute through a 870 nm interference filter using water bath as a heat filter [47].

The light-induced changes that take place on relatively long time scales were studied in the reaction centers from the wild type and a number of mutants. For one-minute illumination times, the formation and recovery kinetic traces were multiphasic (at least 3 components) (Figure 3.8) in the same manner as previously found for reaction centers from the R-26 strain. The behaviour of the reaction centers with regard to the slow rate (k_{slow}) of recovery of the P^+ fell into distinct groups depending upon the mutations present.

A correlation is evident between the midpoint potential of the dimer and the rate of the P^+ recovery in one set of mutants (Figure 3.9). For this reaction, the free energy difference is directly related to the midpoint potential of P, with a correction for the midpoint potential of the exogenous reductant. Assuming very large reorganization energy of at least 1 eV, a linear dependence of log k_{slow} upon the free energy difference is expected from Marcus theory [48]. The observed dependence indicates that in the wild type and these mutants, the process is controlled by the electron transfer rate.

For mutants with the Leu to His at L131 alteration, the relative rate constant $k_{slow}^{mutant}/ k_{slow}^{wt}$ is independent of the driving force thus, the observed rate must be limited by another factor, *e.g.* the rate of protonation and/or the conformational change. Because some of these mutants show a faster rate than other mutants with similar midpoint potentials, the presence of the Leu to His mutation at L131 must result in an increase in the electron transfer rate, so that the electron transfer rate is significantly faster than the observed rate.

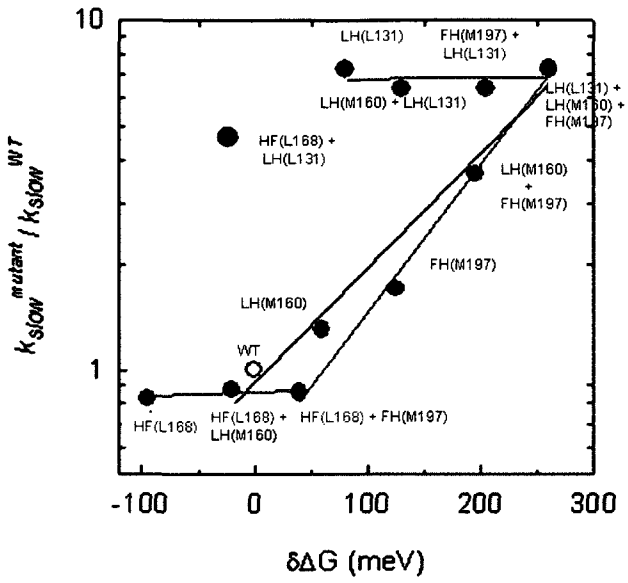

Figure 3.9 Dependence of the rate constant of slow recovery of the oxidized dimer on the difference in driving force between the wild type and 11 hydrogen-bonding mutants in reaction centers. Regression lines were generated through the data points associated with the mutants containing LH(L131) (red), LH(M160) (blue), FH(M197) (magenta) and HF(L168) (green) mutations. The difference in the driving force for the electron transfer between the mutants and the wild type was calculated using the midpoint potentials from [41].

For the R-26 strain without any mutation, the biphasic properties of the optical spectroscopy and proton uptake/release measurements were interpreted by many authors as arising from two different conformations, a dark and light-adapted state [49, 50]. The biphasic behavior was significantly altered in the mutants that contain the LH(L131) mutation, and the observed rate k_{slow} is the same as measured for flash illumination. The presence of the hydrogen bond between the 9-keto group of the L half of the dimer and His L131 appears to prevent the previously proposed conformational change in the vicinity of the dimer. The kinetics of the absorption changes caused by non-saturating illumination were

measured at the $(BChl)_2$ band position (determined from Figure 3.6) in one-one representatives of the two groups of the mutants, wild type and in the LH(L131) mutant at pH 6, where the conformation changes were even more pronounced (Figure 3.10). Similarly, as found at pH 8, the recovery of charge separated states are much faster in the LH(L131) mutant as compared to wild type RC. This indicates that the light-induced conformational changes resulting to longer-lived charge separated states are blocked in the mutants, where the L half of the dimer is immobilized by both hydrogen bonds between the L168 His and the 2 acetyl group and the L131 His and the 9-keto group of the dimer. This structural constrain is in line with the lack of the reverse shift in the Bchl bands in the mutants containing the LH(L131) mutations.

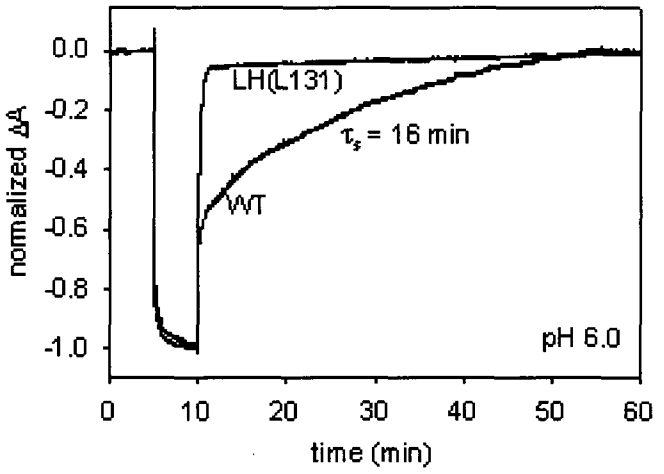

Figure 3.10 Formation and disappearance of the long (5 min) continuous light induced $P^+Q_A^-$ redox states in the reaction centers of wild type and LH(L131) mutant at pH 6 measured at 865 and 870 nm, respectively. Conditions were as follows: 2 μM reaction centers in 15 mM MES (pH 6.0), 0.1% LDAO, 1 mM EDTA, 100 mM NaCl, 100 μM terbutryn. Illumination time: 5 minute through 870±15 nm interference filter using water bath as a heat filter.

Table 3.2 Kinetic and steady state optical spectroscopic parameters of the wild type and 11 hydrogen bonded mutants measured in the reaction centers of *Rb. sphaeroides.*

#	Strain	[a]P pos (nm)	[b]790 pos (nm)	[c]k_{slow} decay x10^2 (s^{-1})
1	HF(L168)	849	790	1.63
2	LH(M160)+HF(L168)	840	788	1.72
3	FH(M197)+HF(L168)	832	790	1.69
W	WILD TYPE	865	790	1.96
4	LH(M160)	862	788	2.56
5	FH(M197)	863	790	3.33
6	FH(M197)+LH(M160)	864	788	7.14
7	HF(L168)+LH(L131)	856	784	13.3
8	LH(L131)	870	784	14.28
9	LH(M160)+LH(L131)	868	781	12.5
10	FH(M197)+LH(L131)	865	782	12.5
11	FH(M197)+LH(M160)+ LH(L131)	865	784	14.28

[a]Position of the Q_Y band of the dimer in the light-minus-dark different spectra of the strains in Q_A active reaction centers (determined from Figure 3.6);

[b]Position of the lower wavelength band of the electrochromic shift on bacteriochlorophyll observed at 790 nm in the light-minus-dark difference spectrum of wild type (data determined from Figure 3.6);

[c]Rate constants of the slowest decaying component of P^+ after 1 minute illumination (determined from Figure 3.8).

Hence, the rate of recovery of the oxidized dimer depends systematically on the protein environment of the dimer. In particular, changes in certain residues appear to prevent a light-induced conformational change that results in a slow recovery and a large proton release [47].

This can also be explained by comparing kinetic traces for LH(L131) and wild type reaction center (Figure 3.10). Since the L half of the bacteriochlorophyll dimer in LH(L131) mutant is fixed, it cannot move with respect to the BChl monomer resulting fast recovery of the oxidized dimer (Table 3.2) as compared to the wild type reaction center.

In summary, by altering the H-bonding pattern near the bacteriochlorophyll dimer, different conformational states can be formed (Figure 3.11). The intermediate state, with a rate constant of 0.1 s^{-1}, was observed in all mutants. This indicates that the formation of this conformational state is due to the conformational changes that are occurring near the quinone side, which was found by many authors [43-46]. The longer lived conformational state was observed upon movement of the monomer followed by the dimer at pH 6 (black squares in Figure 3.11).

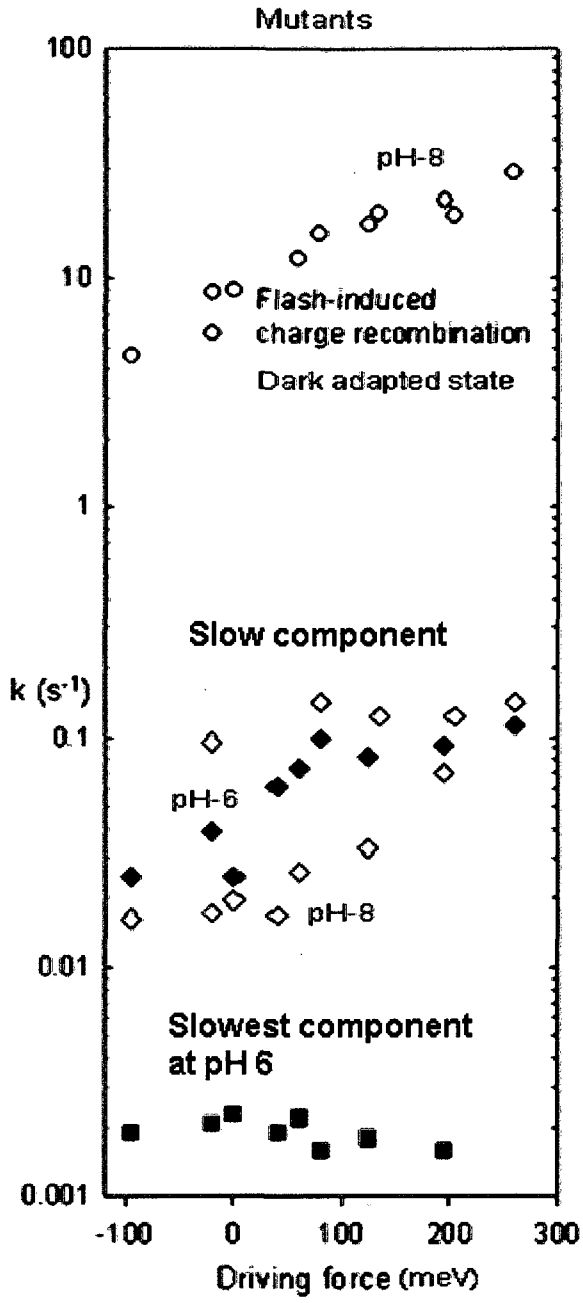

Figure 3.11 Correlation between the rate constants of the kinetic components for the charge recombination from different conformational states due to the genetic alteration of the H-bond pattern of the dimer. Charge recombination from the dark adapted state was measured upon flash excitation (open circles). At pH 8 the conformational change cannot proceed all the way down resulting in rate constants between 10^{-1} and 10^{-2} s^{-1}, (open diamonds), while at pH 6 the recovery rate constants are in the 10^{-3} s^{-1} range (closed squares) with amplitudes varying depending on the mutants.

Chapter 4

Environmental factors affecting the light-induced conformational rearrangements

4.1 Occupancy of the secondary quinone binding site

Formation and recovery of the oxidized dimer was monitored by recording absorption changes at the dimer band position (865 nm). The lifetimes of the charge separated states from the primary (Q_A) and secondary (Q_B) quinone are significantly different [23], which can be studied by using the potent inhibitor terbutryn. Kinetic traces were recorded in LDAO and Triton X-100 detergents in the presence and absence of terbutryn (Figure 4.1).

Kinetic traces in the presence of inhibitor for both detergents are similar to each other but in the absence of inhibitor charge formation and charge recombination are different for different detergents. The formation of a very long lived charge separated state does not depend on the presence of the secondary quinone [23] but its lifetime may be altered.

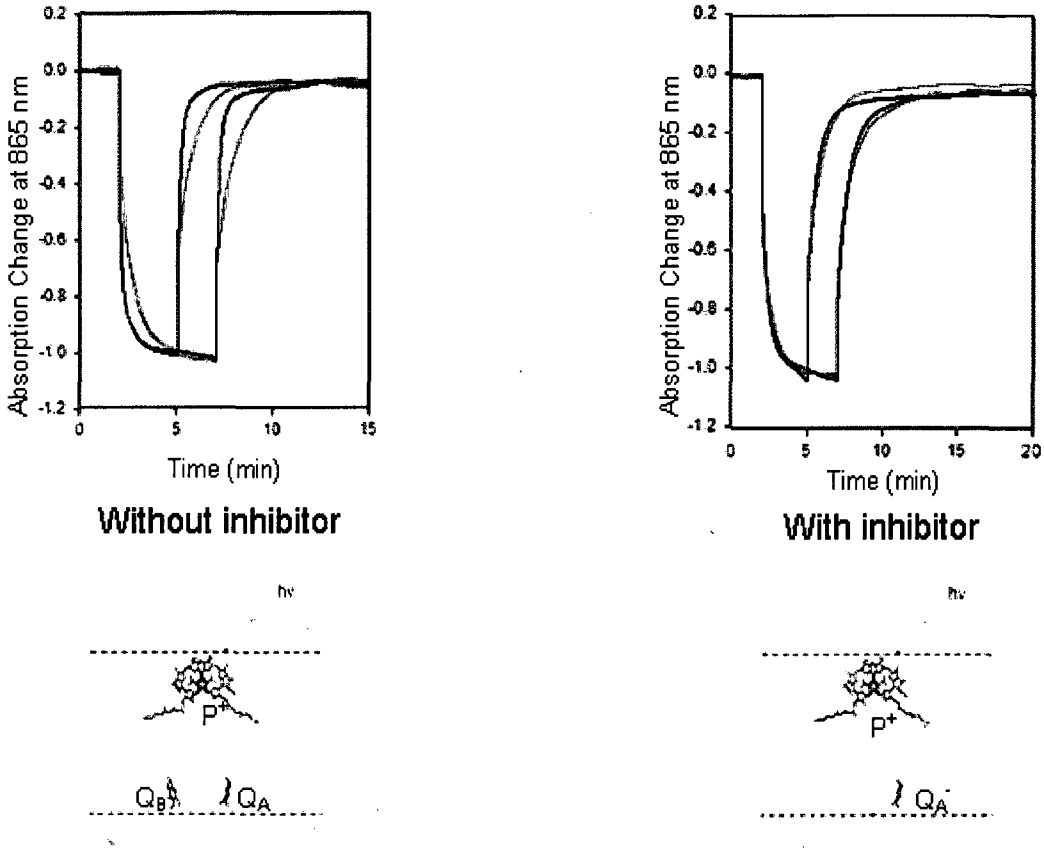

Figure 4.1 Comparison between the kinetic traces for the formation and recovery of the charge separated states from primary (Q_A) and secondary quinone (Q_B). Charge formation and charge recombination in the absence (left side) and presence (right side) of the potent inhibitor (terbutryn) recorded at 865 nm upon prolonged illumination with a non-saturating light source in LDAO (cyan) and Triton X-100 (purple) detergent micelles. In the absence of inhibitor the charge separated state is $P^+Q_B^-$ and in the presence of inhibitor the charge separated state is $P^+Q_A^-$ (schematic representation at the bottom of the kinetic traces). Rate constants of recovering component were 0.013 and 0.014 s^{-1} for LDAO and 0.023 and 0.029 s^{-1} for Triton X-100 without inhibitor but with inhibitor those were 0.021 and 0.023 s^{-1} for LDAO and 0.024 and 0.027 s^{-1} for Triton X-100. Conditions: Kinetic traces were recorded for 1 μM BRC from carotenoidless strain R-26 at pH-8 upon 3 min and 5 min. of illumination with detergent concentration of 1%. A tungsten lamp (120 W) was used as illumination source.

In the presence of a potent inhibitor such as terbutryn, $P^+Q_A^-$ charge separated state was formed. Since the primary quinone (Q_A) is surrounded by the hydrophobic environment, it is not accessible to the external solvent therefore it cannot sense the change in the hydrophobic environment and the kinetic traces were similar in the presence of LDAO and Triton X-100 detergent micelles (Figure 4.1). In the absence of inhibitor the $P^+Q_B^-$ charge separated state was formed. The secondary quinone (Q_B) is accessible to the external environment and therefore can sense the change in the environment and causes different kinetic traces for the charge separation and charge recombination (Figure 4.1).

4.2 Illumination time dependence of the rate constant of the slowest disappearing component

The absorption change at the dimer band position (865 nm) was monitored by varying illumination times. After turning off the light the rate constants of the slowest kinetic component became independent of the illumination time after 30 s, and 2 minutes in LDAO and Triton X-100 detergents respectively for various pH values (Figure 4.2). Upon increasing illumination time only the fraction of the slowest component increases but the rate constant remain independent.

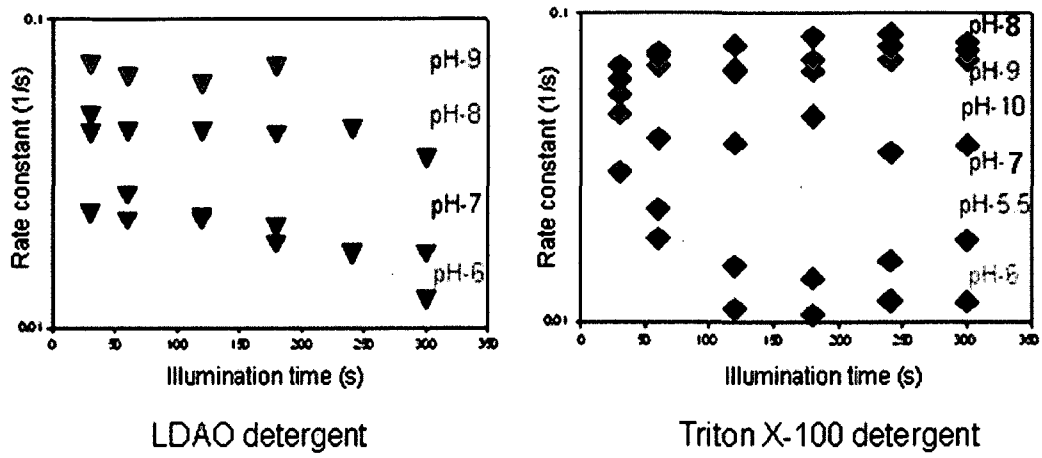

Figure 4.2 Illumination time dependence of rate constant of the recovering component in LDAO and Triton X-100 detergent micelles. Rate constant of the slowest recovering component becomes independent of the illumination time 30 s and 2 min after the illumination in LDAO (left panel) and Triton X-100 detergent micelles (right panel) respectively. Conditions: 1 μM of BRC from carotenoidless strain R-26 in 0.1% LDAO and 0.1% Triton X-100 detergent with 100 μM terbutryn. Tungsten lamp with a power of 120 W was used as illumination source.

Prolonged illumination causes conformational rearrangements, which lead to long lived charge separated states. Charge recombination from $P^+Q_A^-$ to PQ_A is a first order electron transfer process therefore it is independent of illumination time at various pH values. In the case of LDAO detergent micelles the charge separated state goes to the final conformation after a short illumination of 30 s but in the case of Triton X-100 detergent micelles, it takes at least 2 min of illumination to reach the final conformational state down the cascade (Figure 4.2). After 2 min these rate constants of the slowest recovering component become independent of the illumination time because the charge recombination takes place from the same altered conformational state. These rate constants were in the range of 0.01 s^{-1} to

0.1 s^{-1} or in other words the lifetime of these charge-separated states were in the range of 10 s to 100 s and can be altered by altering pH. The rate constant at pH 6 in the presence of LDAO detergent micelles shows moderate dependence on illumination time because of positive head-group charge of the detergent at this pH (pKa ~ 6.6 [22]) which causes readjustment of the α-helices [17, 31].

The pH dependence of these rate constants (Figure 4.3) indicates that for both zwitterionic LDAO and non-ionic Triton X-100 detergents the rate constant increases as pH increases between pH 6 and 10.

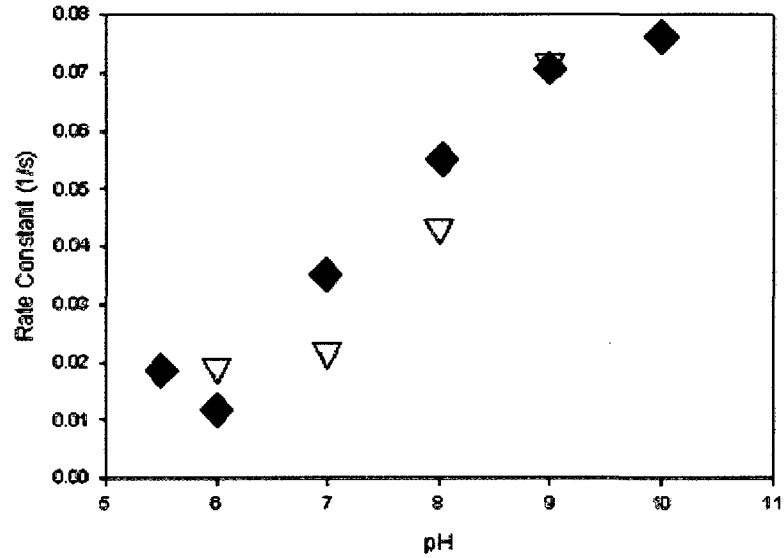

Figure 4.3 pH dependence of the rate constant of the slowest recovering component in LDAO and Triton X-100 detergent micelles. Rate constant of the recovering component increases with increasing pH in LDAO (cyan triangles) and Triton X-100 (purple diamonds) detergent micelles. Conditions: 1 μM of BRC from carotenoidless strain R-26 in LDAO and Triton X-100 detergent with 100 μM terbutryn. Tungsten lamp (120 W) was used as illumination source. The data were taken after 3 minutes of illumination.

In BRC, 158 protonatable residues are present. These residues are near periplasmic or cytoplasmic part of the BRC, which is hydrophilic and accessible to external solvent. The majority of these protonatable residues (58 residues) are acidic residues (Asp, Glu) and have pKa around 6 in the protein environment [22, 51]. At and below pH 6 positively charged residues are higher in number near the cytoplasmic side (quinone side) than the periplasmic side (dimer side), which stabilizes the negative charge on the quinone and causes maximum lifetime for the charge separated state (Figure 4.3).

4.3 Temperature dependence of the charge recombination kinetics of the slowest component

As temperature increases the dimer band position was moved towards the blue. This behavior can be reversed as the temperature decreases (Figure 4.4). At 30° C dimer band shifted to 846 nm at pH-6 and similar band position was observed in the HF(L168) mutant, where introduction of the Phe residue replacing the His removed the H-bond between the L168 and the 2 acetyl group of the dimer (Figure 3.6) [47].

Since the dimer band position in HF(L168) mutant was 849 nm (Table 3.2), the spectral band shift in the $(BChl)_2$ upon increasing temperature can be anticipated as weakening of the hydrogen bond, which is present between the L half of the bacteriochlorophyll dimer and His residue (LH168) in BRC as shown in Figure 4.4. Positive head-group charge of the LDAO detergent at pH 6 causes large difference in overall upward and downward shift of the dimer band position.

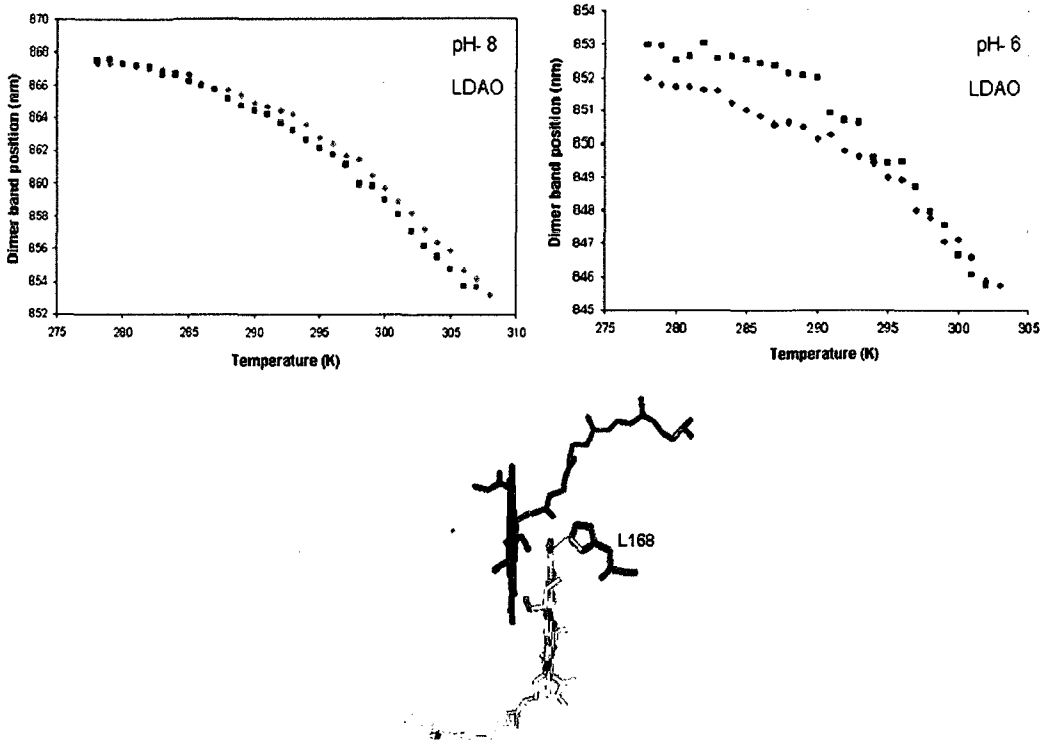

Figure 4.4 Movement of the Bchl dimer band position as a function of the temperature in the carotenoidless R-26 strain. The shift in the band position was found to be reversible at pH 8 and 6 (upward and downward) as temperature changes. At pH-8 $(BChl)_2$ moved from 868 to 853 nm and at pH-6 it moved from 853 nm to 846 nm. Lower panel shows the top view of the L- (yellow) and M half (red) of the $(BChl)_2$ from the wild type BRC. His (LH-168) residue in orange forms hydrogen bond (green dotted line) with L half of the dimer at the 2-acetyl group. The figure was prepared by Pymol software from PDB code: 4RCR.

The kinetic traces at different temperatures were recorded at the dimer band position and analyzed. Activation energies were calculated from the Arrhenius plots of the data for the slowest kinetic component (using Equation 3) (Figure 4.5). They were found to be similar in LDAO and Triton X-100 detergent (Figure 4.6).

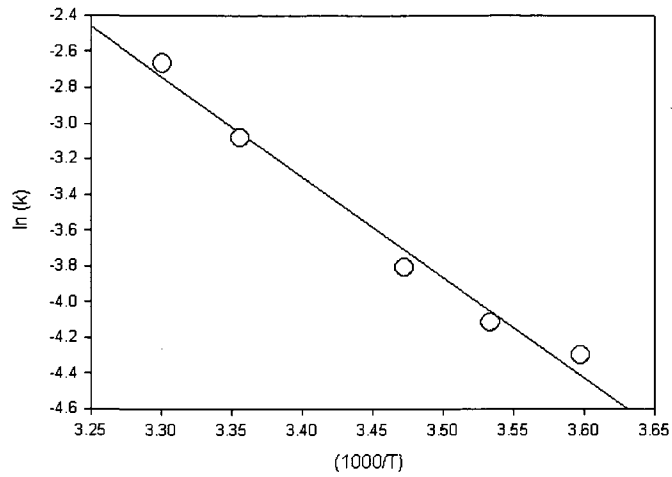

Figure 4.5 Arrhenius plot for charge recombination from BRC incorporated in LDAO detergent micelle upon prolonged illumination. Recovery of the oxidized dimer (865 nm) of BRC incorporated in LDAO detergent micelles was measured at various temperatures. Linear regression was used to best fit the data points and to calculate the activation energy from the slope. The activation energy was found to be 45 ± 3 kJ/mol. Conditions: 1 μM of BRC from carotenoidless strain R-26 in 0.1% LDAO detergent at pH 8 with 100 μM terbutryn and 5 minutes of illumination. Tungsten lamp (120 W) was used as illumination source.

The pH dependence of activation energy for the recovery of the oxidized dimer indicates that pH 6 and 7 have the lowest activation energies for LDAO and Triton X-100 detergents respectively and it increases with pH thereafter (Figure 4.6).

After analyzing Arrhenius plots at different pH values, activation energies were calculated (Figure 4.6). These activation energies have similar trend in the case of LDAO and Triton X-100 detergents but when the temperature dependence was measured in the case of the proteoliposome then the breaking point was observed where the lipid changes from its liquid crystalline phase into a gel phase [52]. The liquid crystalline phase has a similar activation energy to that of the detergents but

the gel phase has a much higher activation energy, indicating a slow process of charge recombination [52].

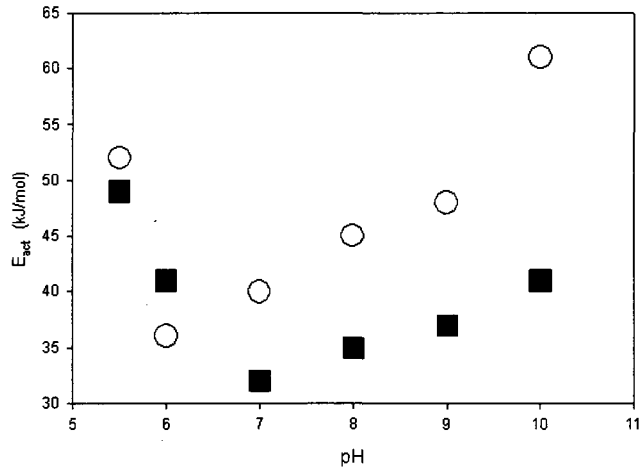

Figure 4.6 pH dependence of activation energy for BRC incorporated into LDAO and Triton X-100 detergent micelles. Activation energy was found to be lowest at pH 6 and pH 7 for LDAO (cyan circles) and Triton X-100 (purple squares) detergent micelles respectively and it increases with pH thereafter. Conditions: 1 μM of BRC from carotenoidless strain R-26 in 0.1% LDAO and 0.1% Triton X-100 detergent micelles with 100 μM terbutryn and 5 minutes of illumination. Tungsten lamp with power of 120 W was used as illumination source.

In BRC's, the majority of the carboxylic amino acids have pKa's around 6 [22]. The carboxylic acid residues near the dimer, upon protonation, destabilize the positive charge on the bacteriochlorophyll dimer. In turn, the positive charge on the dimer lowers the pKa values by releasing protons (Figure 4.7). This effect is pronounced at pH 6 and becomes unaffected at higher and lower pH values therefore the activation energy was lowest at pH 6 and 7 for LDAO and Triton X-100 detergent micelles respectively and increases with increasing pH (Figure 4.6).

As pH increases the amino acid residues near the quinone also deprotonate and destabilize the negative charge on the quinone, which also causes an increase in the activation energy.

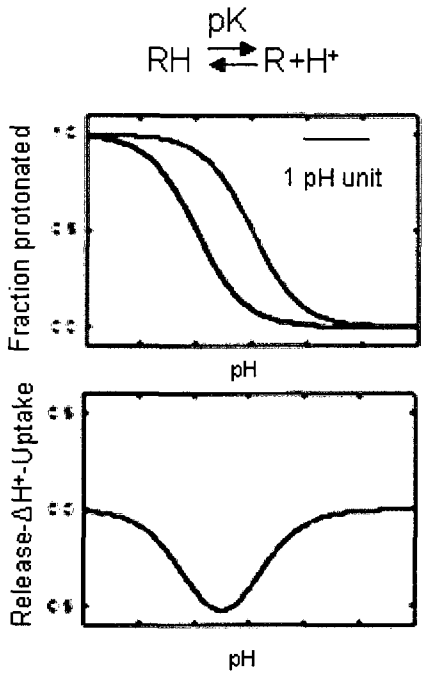

Figure 4.7 Shift of the pK, simulated Henderson-Hasselbalch curve. The presence of a positive charge (*e.g.* on the bacteriochlorophyll dimer) near a protonatable amino acid residue induces a downshift in the pK of a given amino acid (blue curve in upper graph) as compared to its previous (black curve). This shift can be observed as a substoichiometric proton release as the differences between the two Henderson-Hasselbalch curves (lower curve). The effect is mostly observable at pH values between the unaltered and shifted pKs.

The temperature dependence of the charge recombination was measured by using laser flash photolysis and analyzed by Arrhenius plot in order to determine the activation energy of the process upon flash excitation (Figure 4.8), which was found to be 25 ± 8 kJ/mol.

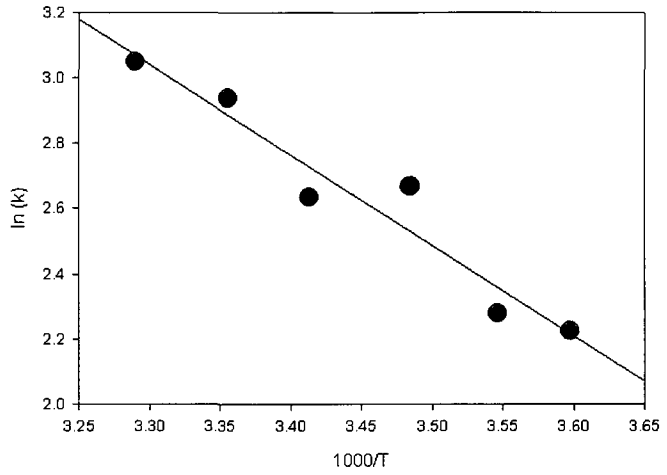

Figure 4.8 Arrhenius plot for charge recombination from the dark adapted state in BRC incorporated in LDAO detergent micelle followed a flash excitation. Recovery of the oxidized dimer (865 nm) of BRC incorporated in LDAO detergent micelles was measured at various temperatures by using Peltier cell upon flash excitation. Linear regression was used to best fit the data points and to calculate the activation energy of 25 ± 8 kJ/mol from the slope. Conditions: 1 μM of BRC from carotenoidless strain R-26 in 0.1% LDAO at pH 8 with 100 μM terbutryn.

The temperature dependence of flash induced charge recombination (Figure 4.8) was explained as a result of different numbers of hydrogen bonds to quinone in the reduced and oxidized states as a result the probability of electron tunneling depends on temperature non-monotonously [53].

4.4 Effect of the bound metal ion on kinetics of the charge recombination

Binding of metal ions (copper, cobalt) to a local protein environment has been shown to modulate the forward electron transfer and the charge recombination [54]. Transition metal ions like Cu^{2+}, Co^{2+} and Mn^{2+} form octahedral structures with water molecules as ligands in solution. When these water molecules are

replaced by amino acid side chains from the macromolecule then binding of this transition metal ion becomes stronger with each binding (Figure 4.9).

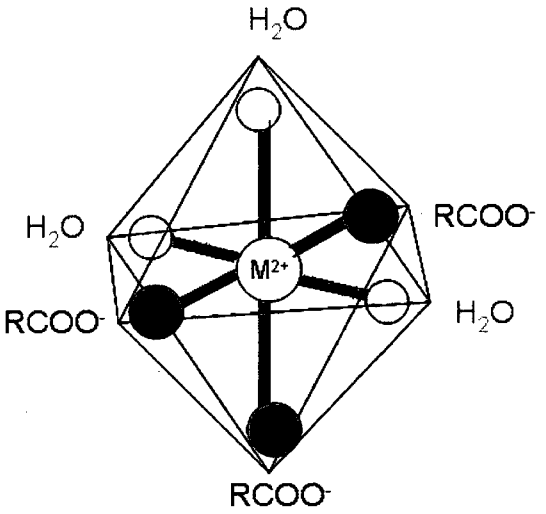

Figure 4.9 Coordination of a metal ion with eight ligands to form octahedral geometry. The central metal ion (M^{2+}) coordinates with water molecules (cyan) in solution but upon availability of negatively charged residues (red) binding becomes stronger. The more negatively charged residues that are available, the stronger the binding will be.

The strongest binding can be achieved if all six water molecules can be replaced with amino acid side chains with the smallest possible distortion from the symmetrical octahedral geometry.

Being divalent these metal ions have less affinity for the binding site that is surrounded by positively charged residues. Bicarbonate can coordinate with metal ions and maximizes the possibility of binding the metal ion to these positively charged binding sites by reducing the net positive charge to zero. Manganese and copper metal ion binding showed a pronounced difference with and without

bicarbonate unlike cobalt metal ions in the rate constant of the slowest recovering component (Figure 4.10).

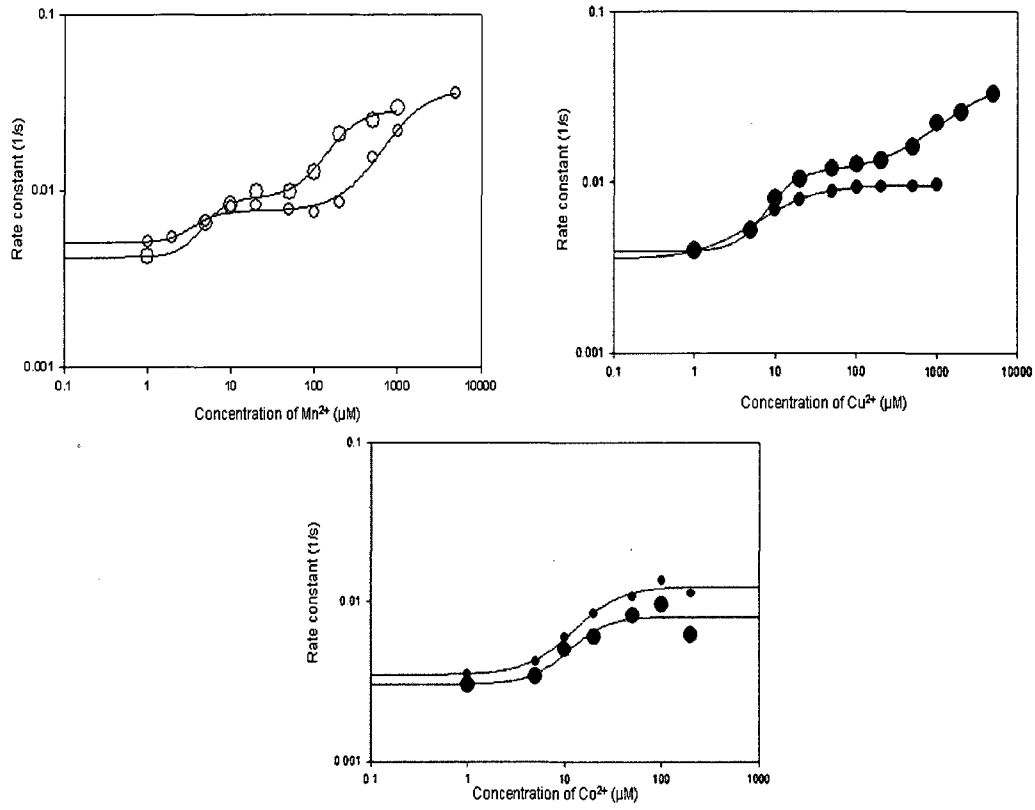

Figure 4.10 Hill plots for the binding of a metal ion to the BRC. Metal ions were titrated in BRC solution. Cu^{2+} (blue) and Co^{2+} (brown) metal ions without bicarbonate show only one binding site and can be best fitted with the Hill equation (Equation 4) to determine the binding constant (Table 4.1) and nature of the binding. Co^{2+} (pink) in the presence of bicarbonate does not show much difference in binding but Mn^{2+} (yellow) and Cu^{2+} (green) show two binding sites and can be best fitted by the summation of two Hill equations. Gray symbols represent Mn^{2+} without bicarbonate and drawn lines are the best fit to the measured data points (Equation 4). Conditions: 1 µM BRC from carotenoidless strain R-26 at pH 8 with 100 µM terbutryn and 5 min of illumination with a tungsten lamp (120 W). The BRC was dialyzed for 24 hours to remove EDTA in order to prevent chelation of metal ion.

The data was analyzed by using the Hill equation (Equation 4), which tells about the co-operative nature of binding [55, 56]. Analyzed results are tabulated in Table 4.1.

Table 4.1 Hill constants (n_H) and binding constants (K) for manganese, cobalt, and copper metal ion with and without bicarbonate determined from Hill plots (Figure 4.10). Figures in red are much higher values than unity.

Metal ion	Mn^{2+}		Co^{2+}		Cu^{2+}	
	n_H	K (μM)	n_H	K (μM)	n_H	K (μM)
With HCO_3^-	2.9±0.1 2.1±0.67	5±0.6 182±32	2.2±0.9	13±3	2.4±0.16 1.14±0.21	9.7±0.5 1750±243
Without HCO_3^-	3±0.2 1.6±0.43	3.7±0.23 1042±105	1.8±0.7	17±4	1.2±0.75	9.1±0.4

Binding of the metal ion inhibits the formation of long lived conformational states as it accelerates the rate constants of the recovering component (Figure 4.10). After fitting these data by using the Hill equation (Equation 4), binding constants and Hill constants were obtained as indicated in Table 4.1.

The Hill constant tells about the cooperative binding of the metal ion to a macromolecule. If the Hill constant is less than unity then there is negative cooperative binding which means binding of a metal ion disfavors the subsequent binding of metal ions. If the Hill constant is more than unity then there is positive

cooperative binding which means binding of a metal ion favors the binding of subsequent metal ions to the macromolecule. If the Hill constant is equal to unity then it is non-cooperative binding [56]. Figures in red (Table 4.1) are much higher than unity indicating positive cooperative binding, which can be interpreted as two binding sites in case of manganese ion with and without bicarbonate and only with bicarbonate in case of copper ion within the concentration range studied. High binding site affinity or first binding site causes an increase in the rate constant of the slowest recovering component from 0.001 to 0.01 s^{-1} indicating inhibition of the long lived conformational state. While the low binding site affinity or second binding site in the presence of bicarbonate further inhibits the formation of 100 s component in the case of copper and manganese. On the other hand, in the case of cobalt, bicarbonate does not facilitate the binding to the low affinity site. This can be interpreted as the difference in geometry. Cobalt and copper have known binding sites near the secondary quinone [54] in accordance with high affinity binding sites, which do not inhibit the formation of the 100 s component (Figure 4.10). The low binding site affinity inhibits the formation of this conformational state indicating the possible binding site near the bacteriochlorophyll dimer, which alters the local electrostatics and hence the interaction between the $(BChl)_2$ and BChl monomer. Manganese has at most 7 binding sites in the reaction center as reported earlier [57].

4.5 Effect of the detergent concentration on kinetics of the charge recombination

Purification and incorporation of BRC's was done in 0.1% LDAO detergent at pH 8. Varying amounts of quinone were removed by incubating the BRC's for 3-6 hours at 25° C in the presence of different amounts of LDAO (1-4%) and o-phenanthroline [58]. Therefore, two different detergents were studied to analyze the effect of detergent concentration on the recovery kinetics of the oxidized dimer after prolonged illumination. After analyzing the kinetics of the slowest kinetic component it was found that at pH 8, for both LDAO and Triton X-100 detergents, the rate constants were almost independent of the detergent concentration provided that it was above the c.m.c. (Figure 4.11). In contrast, at pH 6 the ionic detergent LDAO and the nonionic Triton X-100 showed opposite trends in the detergent concentration dependence of the rate constant of the slowest recovering component. The LDAO, which has a pKa of 6.6 [22], and is therefore slightly positively charged at pH 6, showed a markedly accelerated recovery of the dimer upon increasing detergent concentration. The nonionic Triton X-100 detergent on the other hand moderately decreased the value of the rate constant of the slowest component upon increasing concentration. The opposite behaviour of these two different detergents indicates that the charges, and thus the charged amino acid residues, near the dimer and the quinone play a key role in the formation and disappearance of the light-induced conformational substates.

In the wild type reaction center, the carotenoid is present near the $BChl_B$ to prevent photo-degradation of the pigments [59]. In the carotenoidless reaction center (R-26) this place was filled by the detergent molecule [59] (Figure 4.12) and moreover $BChl_B$ is solvent accessible [60]. Triton X-100 is a non-ionic detergent and hence cannot alter the electrostatic interaction between the bacteriochlorophyll dimer and the bacteriochlorophyll monomer, therefore at pH 8 the rate constants of the slowest recovering components became independent of the concentration of detergent (Figure 4.11).

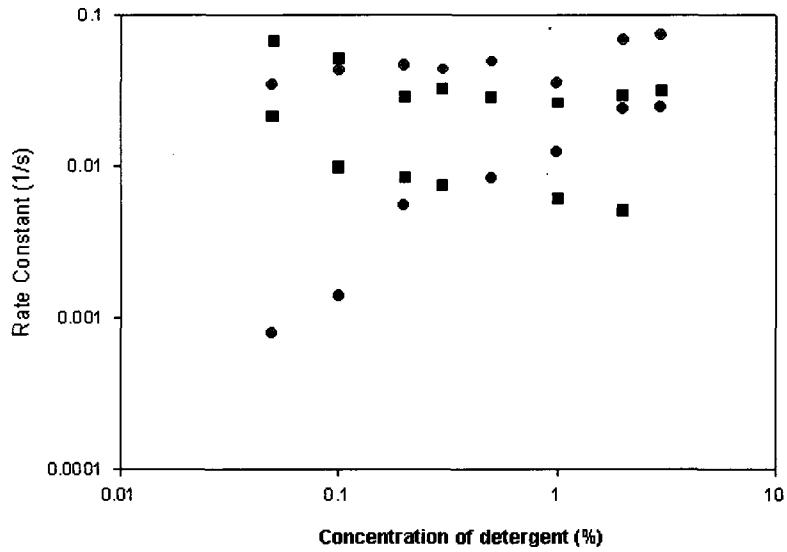

Figure 4.11 Rate constants of the recovery of the oxidized dimer as a function of detergent concentration. Detergents were titrated in the BRC solution. LDAO (green circles) and Triton X-100 (brown squares) at pH 8 show independent nature of rate constant as a function of detergent concentration but Triton X-100 at pH 6 (black squares) show moderate dependence. LDAO at pH 6 (red circles) was found to be markedly dependent on concentration; increasing concentration accelerates the recovery of oxidized dimer. Conditions: 1μM BRC from carotenoidless strain R-26 at pH 6 and 8 with 100 μM terbutryn and 5 min of illumination. Tungsten lamp (120 W) was used as illumination source.

LDAO is a zwitterionic detergent and at pH 8 it has a zero net charge in solution [21], therefore an incoming LDAO molecule cannot alter the bacteriochlorophyll dimer and monomer interaction. But it has a net positive charge at pH 6, which alters the permanent dipole-induce dipole interaction of bacteriochlorophyll dimer and monomer respectively resulting in inhibition of the formation of the long lived conformational state (1000 s component) at higher concentrations.

At very high concentration of LDAO detergent the rate constant of the slowest recovering component became lower, which resembled the rate constant of the slowest recovering components in Figure 4.1 in the presence of the inhibitor. This can be explained as at very high concentration of LDAO, the primary quinone becomes accessible to the solvent [58]. While Triton X-100, at pH 6, moderately altered the rate constants as the concentration was increased and it is was as effective as LDAO in accessing the primary quinone.

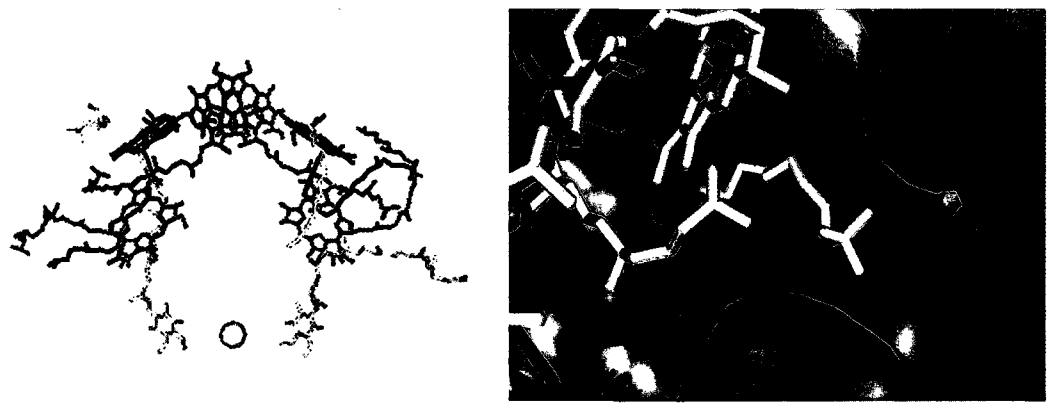

Figure 4.12 Cofactors of the BRC with LDAO detergent molecule. Left: BRC cofactors and the LDAO detergent molecules (pink) near the $BChl_A$ and $BChl_B$. LDAO detergent molecule can go closer to $BChl_B$ because it is solvent accessible **Right:** Position of LDAO molecule (white) near $Bchl_B$ (yellow) in the BRC. Figure was prepared by Pymol software from the PDB file 1RG5.

This was also verified by analyzing the light-minus-dark difference spectra for the detergent concentrations as determined earlier for the spectral band shifts (data not shown). From the analysis, it was found that $BChl_A$ moved from 790 to 788 nm and Bpheo moved from 760 to 758 nm but the major change was observed in $BChl_B$, which moved from 810 to 796 nm for a 3% concentration of LDAO at pH 6. This indicated that the incoming detergent molecule was altering the local electrostatics near $BChl_B$ and inhibiting the formation of the long lived conformational state.

4.6 Ionic strength dependence

In order to investigate the role of charge-charge interactions for the conformational changes, the ionic strength dependence was studied to screen these interactions. Increasing ionic strength caused an increase in the rate constant up to 20 mM salt concentration but after that it became independent of the ionic strength. The rate constant of the slowest recovering component was lowest in zero ionic strength but at higher ionic strength all charge-charge interactions were screened and the rate became become independent of the ionic strength (Figure 4.13).

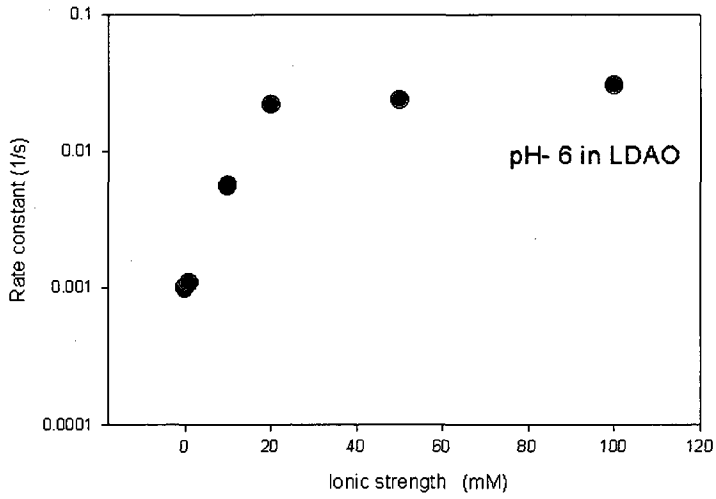

Figure 4.13 Ionic strength dependence of the rate constant of the recovering component. Upon increasing salt concentration the rate constant of the recovering component accelerates and after 20 mM of salt concentration the rate constant remained unaltered. Conditions: 1 μM of BRC from carotenoidless strain R-26 at pH 6 with 100 μM terbutryn and 5 min of illumination. Sodium chloride was used to increase the ionic strength. Tungsten lamp (120 W) was used as illumination source.

The dipole-dipole interactions between the dimer and the monomers are important as far as conformational changes are concerned. After screening the charge-charge interaction with sodium chloride salt, the rate constants of the slowest recovering component became faster, this was studied by ionic strength dependence.

4.7 Effect of the excitation wavelength and excitation intensity

For all measurements the same tungsten lamp was used with a power of 120 W but it was found that the kinetics of the charge recombination was not dependent

upon the light intensity (Figure 4.14B). In contrast, this kinetic of charge recombination varies depending on excitation wavelength (Figure 4.14A).

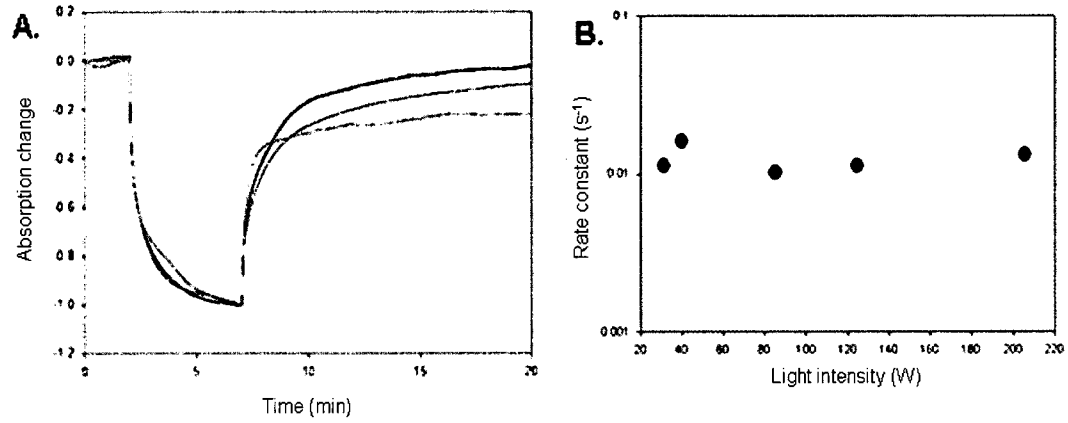

Figure 4.14 A. Wavelength dependence on the recovery of oxidized dimer monitored at 865 nm. Blue trace was recorded with white LED as illumination source, black trace was recorded with tungsten lamp as illumination source, and red trace was recorded by using band pass filter at 865 nm. **B. Rate constants of slowest recovering component as a function of light intensity.** The intensity of illumination source was altered by increasing power of the source. Conditions: 1 μM of BRC from carotenoidless strain R-26 in LDAO detergent with 100 μM terbutryn at pH 8 with 5 min of illumination.

The rate constants of the charge recombination were independent of the intensity of illumination source (Figure 4.14B). At high intensity the B-side electron transfer was promoted by absorbance of multiple photons [61] but in the presence of an inhibitor (terbutryn) $Bpheo_B$ was reduced without altering the kinetics of the A-side charge separated state. As the intensity of the illumination source was increased, the charge separated state was populated faster *i.e.* dark adapted state but the charge recombination took place from the same altered conformational state. This charge recombination was found to be dependent on excitation wavelength (Figure 4.14A) due to either excitation wavelength dependent

photochemistry or of special heterogeneity in the reaction center population, where the charge separated state can be formed due to the oxidation of the monomer A or the bacteriopheophytine A [61]. If the bacteriochlorophyll was excited directly by 865 ± 20 nm then rate of the charge recombination was slowest. The spectrum from the tungsten lamp has some emission in near infra-red region which is closer to the bacteriochlorophyll dimer absorption band therefore it gives slower charge recombination than that of illuminated by white LED, which does not have emission in the near infra-red region.

4.8 BRC as a biocapacitor

In Nature, the charge recombination from the primary quinone takes place in 100 ms in the BRCs (Figure 4.15A). Upon prolonged illumination this charge recombination can be extended up to several minutes in the presence of detergent micelles (Figure 4.15B). Lower temperatures in case of the detergent micelle, do not cause a significant difference in the rate constant of charge recombination; it indeed recovers within 30 minutes. In the gel phase of DLPC liposomes the charge separated state can be further extended up to more than 9 hours *i.e.* 3 million times slower charge recombination compared to in Nature [52] (Figure 4.15C). The hydrophobic mismatch causes the overall upward shift in the DLPC phase transition temperature from 0 to 10° C.

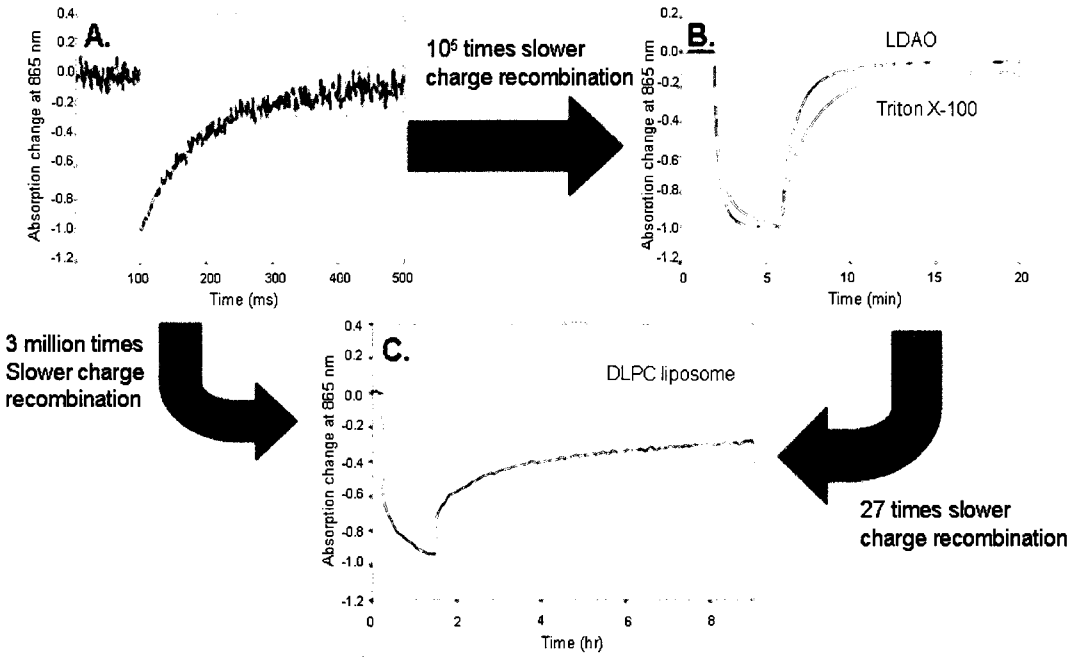

Figure 4.15 Recovery of the oxidized primary donor of the R-26 strain monitored at 865 nm under certain conditions. A. Lifetime of primary charge separated state was measured by laser flash photolysis (~ 100 ms) at room temperature. **B.** Upon prolonged non-saturating illumination of the BRC incorporated in a detergent micelle environment, charge recombination was extended up to several minutes at room temperature, which has a 10^5 times slower charge recombination. **C.** In the gel phase of DLPC the same charge separated state was extended up to several hours at 8° C, which is 3 million times slower charge recombination. Figure was taken from reference 52.

So, upon external illumination of the BRC, a charge separated state can be formed, which has an altered conformation with an extended lifetime. These charges are separated by the hydrophobic core of environment with dielectric constant ~ 4. Since these charges can be kept apart for an extended period of time, this photosynthetic machinery can be used as biocapacitor (Figure 4.16).

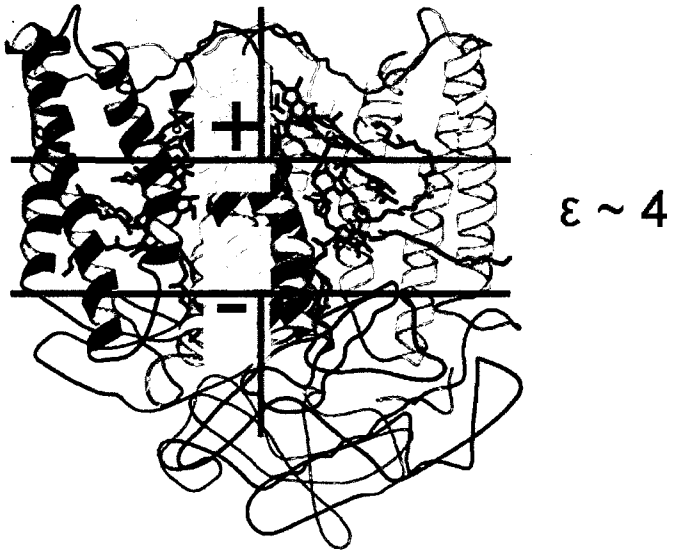

Figure 4.16 Bacterial reaction center as a biocapacitor.

In order to discharge this biocapacitor rapidly, a pH jump can be used. Since, pH 6 has the maximum effect compared with the higher pH values, during the rapid discharge pH can be changed from 6 to 10 (Figure 4.17). Upon change in the pH, the majority of the amino acid residues get deprotonated, disfavoring the charge separated state which causes rapid charge recombination. This can happen rapidly in the presence of detergent micelles because change in pH can easily be sensed by the protein but in case of liposome it takes a few hours for the protein to sense the change in pH due to the random orientation of protein inside the liposome and it also takes few hours for the hydroxyl ion to penetrate through the membrane (Figure 4.18).

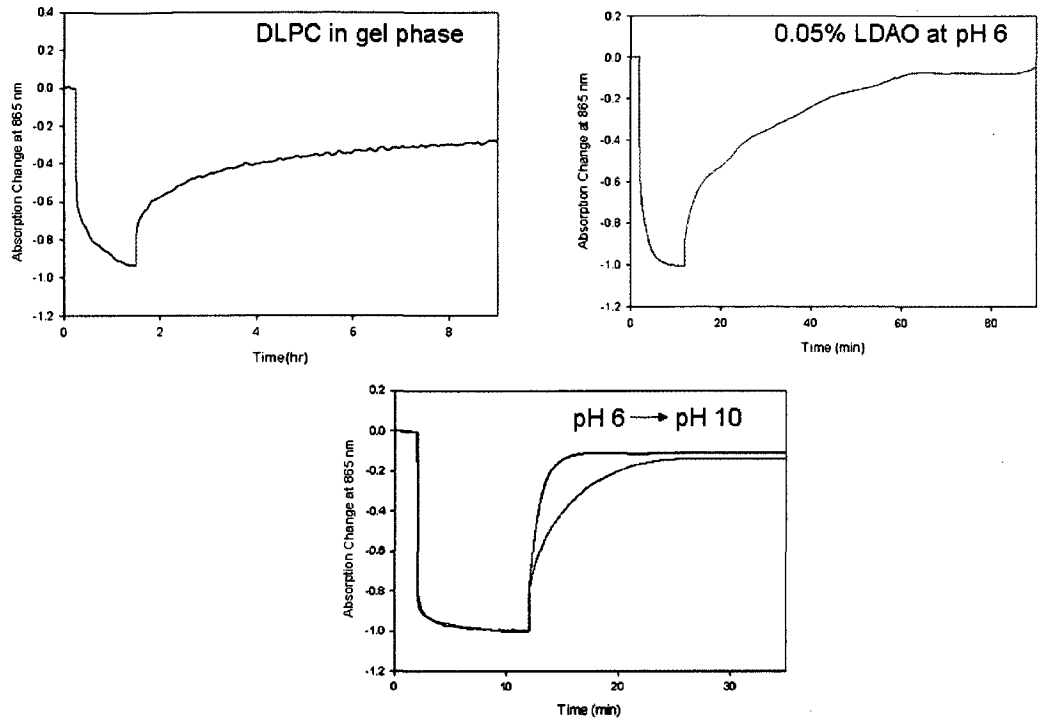

Figure 4.17 Discharging of a biocapacitor by a pH switch. A. Longest kinetic trace recorded in the gel phase of DLPC liposome at 8° C, which takes 90 minutes of illumination for saturation. Figure was taken from the reference 52. **B.** Longest kinetic trace in the presence of 0.05% LDAO detergent micelle environment, which takes 10 minutes of illumination for saturation. **C.** pH jump from 6 to 10 after the illumination causes fast charge recombination.

Charging and discharging of the biocapacitor is faster in the case of the detergent micelles than that of in the liposomes (Figure 4.17), therefore detergent micelles are a more effective environment for a biocapacitor where a pH switch acts as a better tool for rapid discharge. In solution, BRC's have random orientation and for biocapacitor the charge pairs should be oriented properly. Therefore, to obtain proper orientation of the BRC micelles in the solution, electric field can be applied.

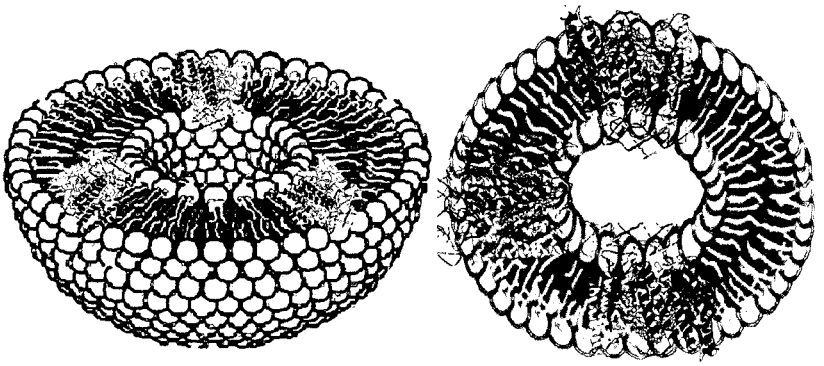

Figure 4.18 Random orientation of BRC in the liposome. Cytoplasmic side of the BRC may be oriented either inside the liposome or outside the liposome.

In summary, a cumulative figure can be prepared from all the factors that affect the formation of different conformational states. For simplicity only Figure 4.2, 4.3, and 4.11 were combined to emphasize different conformational states (Figure 4.19) that can be formed between 0.1 to 0.001 s^{-1} by altering the local electrostatics near the dimer. The conformational rearrangements are sensitive to various different parameters like illumination time, pH, concentration and head-group charge of the detergent, temperature, hydrophobic environment, bound metal ion etc.

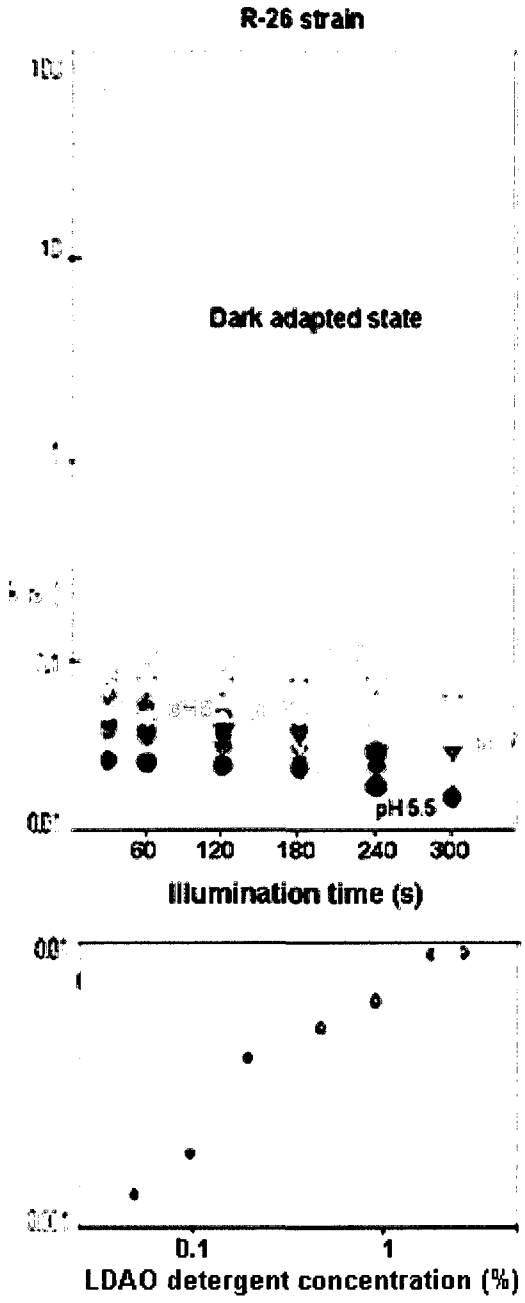

Figure 4.19 Cumulative figure for the environmental factors that form different conformational states upon prolonged illumination. Triangles and circles represent the illumination time dependence in the presence and in the absence of the potent inhibitor terbutryn at different pH values. The red circles at the bottom represent LDAO concentration dependence at the pH 6. At 0.05% of LDAO concentration the slowest conformational state was formed.

Chapter 5

Conclusion

Upon illumination, instant charge separated states are formed (P^+Q^-) as shown symbolically by a rectangular shape for the RC in Figure 5.1B. This is attributed to the charge recombination of the dark adapted conformation, with a 1 s to 100 ms lifetime, depending on occupancy of the secondary quinone binding site. Upon prolonged illumination these charge separated states undergo slow conformational rearrangements to form altered light adapted conformations as shown symbolically by the ellipses or circles (Figure 5.1B). These conformational changes take place to different extents with rate constants of 0.1 s^{-1} to 0.001 s^{-1} between the dark adapted (rectangle) and fully light adapted states (circle). Different conformational states can be formed by altering the H-bonding pattern (Figure 5.1A) or local electrostatics (Figure 5.1C) near the dimer. Hence, the mutant study and other environmental factors' study can be correlated and put in the context of the minimal model of different conformational states.

In the case of mutants that lack LH(L131) H-bonding, and in the case of other environmental factors which do not alter the dipole-dipole interaction between the dimer and monomer, evolution of the slowest kinetic component was observed.

These extended lifetime charge separated states can be attributed to the conformational rearrangements in the BRC, which involves the movement of the bacteriochlorophyll monomer upon illumination followed by the movement of the bacteriochlorophyll dimer. The movement of the bacteriochlorophyll dimer can be

altered by changing various parameters, which help or hinder the charge-charge interactions for its movement resulting in different lifetimes. With these systematic changes, the lifetimes of the charge separated states were increased by 5 orders of magnitude.

The most favorable conditions to increase the lifetime of charge separated state are pH 6 with 0.05% of LDAO detergent with no EDTA in BRC protein. The research effort presented here was aimed not only at controlling the storage of the electrical energy (increasing the lifetimes) of the proposed biocapacitor but also ascertaining that a rapid discharge of it can be induced by a pH jump.

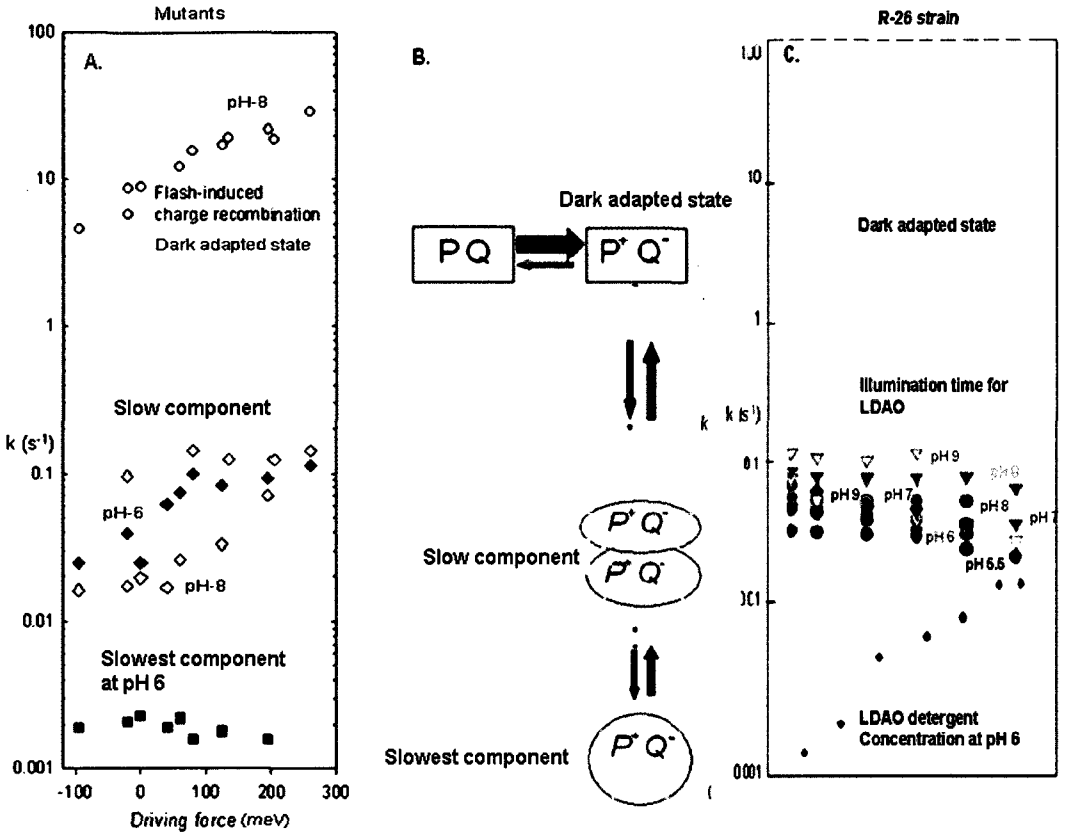

Figure 5.1 Comparison of different conformational states in the mutants and R-26 strain to the minimal model of the light-induced conformational changes. The conformational changes can take place to different extents with rate constants of ~0.1 s^{-1} to ~0.001 s^{-1} between the dark adapted (rectangle) and fully light adapted (circle) states, depending on various factors, such as mutations, pH, ionic strength, illumination time, detergent concentration, Q_B occupancy etc.(Panel A and C). In some cases the conformational changes can only go up to the intermediate states represented by ellipses between dark and light adapted states in our model (Figure 5.1 scheme) but in case of the use of the lipid environment it can go down further. The extent of the conformational changes were monitored by the kinetic analyses of the light-induced absorption changes.

Chapter 6

Future work

This project can further be extended in order to increase the lifetime of the charge separated state in detergent micelles by-

i. Increasing viscosity upon light-induced conformation. In the carotenoidless R-26 strain the $BChl_B$ is solvent accessible so, increase in viscosity by titrating glycerol can inhibit the back movement of the dimer and the monomer that may lead to longer lifetimes of the charge separated states. In recent works, glycerol molecule was also found near the $BChl_A$ as show in Figure 6.1 below.

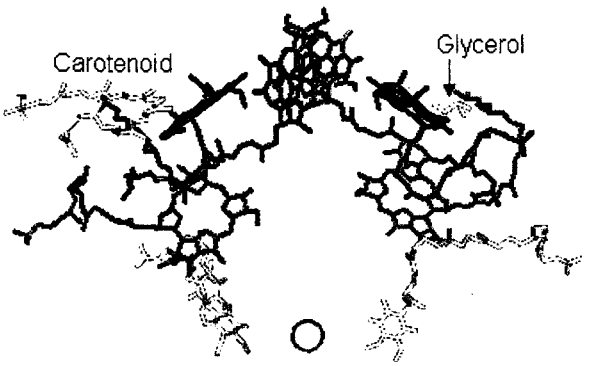

Figure 6.1 The wild type BRC with the carotenoid pigment near the $BChl_B$ and glycerol molecule (pink) near the $BChl_A$. Figure was prepared by Pymol software from PDB code: 2UWW.

ii. Titrating the metal ion in the BRC sample after the light-induced conformational rearrangement to change local electrostatics. If conformational rearrangements facilitate binding of the metal ion near the

dimer then slowest conformational state can be formed by inhibiting back movement of the dimer and monomers.

iii. Using different composition of detergents because use of more than one detergent causes different conformational changes in the BRC protein to compensate for the hydrophobic mismatch.

References

[1] Bacon Ke, *Advances in photosynthesis*, **chapter 11**, *10*, 199-212.

[2] Allen *et al. PNAS*, **1987**, *84*, 6162-6166.

[3] Allen *et al. PNAS*, **1987**, *84,* 5730-5734.

[4] Komiya *et al.* (PDB code: 4RCR) *PNAS*, **1988**, *85,* 7993-7997.

[5] McPherson *et al. BBA*, **1990**, *1016*, 289-292.

[6] Paddock *et al. PNAS*, **1989**, *86*, 6602-6606.

[7] Paddock *et al. Biochemistry*, **1994**, *33*, 734-745.

[8] Takahashi and Wraight, *Biochemistry*, **1991**, *31*, 855-866.

[9] Paddock *et al. PNAS*, **1990**, *87*, 6803-6807.

[10] Takahashi *et al. BBA*, **1992**, *1020*, 107-111.

[11] Takahashi *et al. Biochemistry*, **1992**, *31*, 855-866.

[12] McPherson *et al. Biochemistry*, **1994**, *33*, 1181-1193.

[13] Graige *et al. JACS*, **1996**, *118*, 9005-9016.

[14] Camara-Artigas *et al. PNAS*, **2002**, *99,* 11055-11060.

[15] Paddock *et al. Biochemistry*, **2006**, *45,* 14032-14042.

[16] Axelrod *et al. Photosynthesis Research*, **2005**, *85,* 101-114.

[17] Muh *et al. Biochemistry*, **1997**, *36*, 4155-4162.

[18] Berry *et al. Photosynthesis Research*, **2004**, *81*, 251–275.

[19] Roth *et al. Biochemistry*, **1991**, *30,* 9403-9413.

[20] Milton J. Rosen, *Surfactants and Interfacial Phenomena,* **2004**, *3*, 105-136.

[21] Piazza *et al. Phys. Rev. Lett.*, **2003**, *90,* 208101.

[22] Kalman *et al. Biochemistry*, **1997**, *36*, 4489-4496.

[23] F. van Mourik *et al. BBA*, **2001**, *1504,* 311-318.

[24] Trotta *et al. Material Science and Engineering C,* **2002**, *22,* 263-267.

[25] Sperotto and Mouritsen, *Biophys. J.* **1991**, *59*, 261-270.

[26] Sperotto and Mouritsen, *Eur. Biophys. J.* **1988**, *16*, 1-10.

[27] Dumas *et al. FEBS letters*, **1999**, 458, 271-277.

[28] Bowie, *J. Mol. Biol.* **1997**, *272*, 780-789.

[29] Yeates *et al. PNAS*, **1987**, *84*, 6438-6442.

[30] Bowie, *Nature*, **2005**, *438*, 581-589.

[31] Muh *et al. Photosynthesis Research*, **1998**, *55,* 199-205.

[32] Kleinfeld *et al. Biochemistry*, **1984**, *23*, 5780-5786.

[33] Clayton *et al. Photosynthesis Research*, **2000**, *73,* 63-71.

[34] Muller *et al. BBA*, **1991**, *1098*, 1-12.

[35] Maroti and Wraight, *Progress in Photosynthesis Research*, **1987**, *2*, 401-404.

[36] Williams *et al. Research in Photosynthesis,* **1992**, *1*, 377-380.

[37] Mattioli *et al. Biochemistry*, **1994**, *33,* 1636-1643.

[38] Ivanich *et al. Biochemistry,* **1998**, *37,* 11812-11820.

[39] Williams *et al. Research in Photosynthesis* (Murata, N., Ed.), **1992**, *1*, 377-380, Kluwer Academic Publisher, Dordrecht, The Netherlands.

[40] Murchison *et al. Biochemistry*, **1993**, *32,* 3498-3505.

[41] Lin *et al. PNAS,* **1994**, *91,* 10265-10269.

[42] Nabedryk *et al. Biochemistry*, **1993**, *32,* 13879-13885.

[43] Xu and Gunner, *Biochemistry*, **2001**, *40*, 3232-3241.

[44] Tiede *et al. Biochemistry*, **1996**, *35*, 10763-10775.

[45] Li *et al. Biochemistry*, **1998**, *37*, 2818-2829.

[46] Graige *et al. PNAS*, **1998**, *95*, 11679-11684.

[47] Deshmukh *et al.* To be submitted to Biophysical Journal.

[48] Marcus and Sutin *BBA,* **1985**, *811*, 265-322.

[49] Shopes and Wraight, *BBA*, **1986**, *848*, 364-371.

[50] Debus *et al. Biochemistry*, **1995**, *24*, 2488-2500.

[51] Beroza *et al. Biophys. J.* **1995**, *68*, 2233-2250.

[52] Kai Tang, *Hydrophobic Mismatch Influencing the Structure-Function Relationship of the Reaction Center from Photosynthetic Bacterium Rhodobacter sphaeroides*, **2008**, *Master's Thesis*, Concordia University.

[53] Krasilnikov *et al. BBA*, **2007**, *1767,* 541-549.

[54] Utschig *et al. Biochemistry*, **2001**, *40,* 6132-6141.

[55] Shih and Been, *The EMBO Journal*, **2001**, *20*, 4884-4891.

[56] van Holde, Curtis Johnson, and Shing Ho, *Principles of Physical Biochemistry*, **Chapter 14**, *2*, 605-659.

[57] Kalman *et al. Biochemistry*, **2003**, *42,* 11016-11022.

[58] Okamura *et al. PNAS*, **1975**, *72*, 3491-3495.

[59] Yeates *et al. PNAS*, **1988**, *85,* 7993-7997.

[60] Maroti *et al. BBA*, **1985**, *810,* 132-139.

[61] Lin *et al. J. Phys. Chem. B*, **1999**, *103,* 4757-4763.